

1

AD-A192 107

DTIC

Remote Sensing of Acoustic Properties of Shallow Water Sediments: A Review

DTIC
ELECTE
MAR 09 1988
S D
a H

APL-UW 8711
September 1987

DISTRIBUTION STATEMENT A

Approved for public release;
Distribution Unlimited

Contract N00014-84-K-0646/A00004

88 2 23 09 6

Acknowledgments

This work resulted from an Office of Naval Research contract for which Dr. J. A. Mercer and I were coprincipal investigators. Dr. Mercer kindly attended to coordinative functions that accompanied the preparation and publication of this report. The ONR Contract N00014-84-K-0646/A00004 was supported by Dr. R. M. Fitzgerald, ONR Code 1125AO.

Special thanks go to the successive Directors of the Applied Physics Laboratory, Drs. S.R. Murphy and R.C. Spindel, for their encouragement and support, and especially to Dr. Spindel for his thorough review and suggestions.

I am grateful to the following for technical assistance and for permission to reprint freely their material in this report: Dr. T. Yamamoto, Mr. A. Turgut, Mr. M. Badiy, and Drs. G. V. Frisk, J. F. Lynch, and S. D. Rajan.

I also wish to thank the following for permission to reprint figures and tables from their published work: C. Conner, R. M. Holt, J. M. Hovem, F. B. Jensen, A. Nagl, D. Rauch, B. Schmalfeldt, H. Schmidt, J. Syrstad, G. J. Tango, M. Trevorow, H. Uberall, and M. F. Werby.

ABSTRACT

A review is presented of remote sensing methods and associated inverse procedures for obtaining the acoustic properties of sediments in shallow water. The properties of interest are the vertical profiles of density, compressional wave velocity and attenuation, and shear wave velocity and attenuation. For compressional waves, the remotely sensed information required is the modal reflection coefficient of the seabed, usually expressed in terms of the depth-dependent Green's function at specific locations in the water column. For shear waves, information about the Scholte and Rayleigh interface waves on the seabed is necessary. Also reviewed are methods for remote sensing of the Biot geophysical parameters. shear modulus, permeability, and porosity, from which geoaoustic properties can be derived.



Accession For	
NTIS GRA&I	<input checked="" type="checkbox"/>
DTIC TAB	<input type="checkbox"/>
Unannounced	<input type="checkbox"/>
Justification	
By	
Distribution/	
Availability Codes	
Dist	Avail and/or Special
A-1	

TABLE OF CONTENTS

	<i>Page</i>
I. INTRODUCTION	1
II. COMPRESSIONAL WAVE PROPERTIES	3
A. Introduction	3
B. Inverse Methods	3
1. Plane Wave Reflection Coefficient versus Angle of Incidence	3
Catholic University (CU) method of inversion	4
2. Depth-Dependent Green's Function	5
3. NORDA Method	10
III. SHEAR WAVE PROPERTIES	11
A. Introduction	11
B. Seismic Interface Waves	11
C. Dispersion of Interface Waves	12
D. Sediment Shear Properties	16
E. Schmidt's Numerical Method	21
IV. BIOT GEOPHYSICAL PARAMETERS	24
A. Introduction	24
B. Synthetic Seismograms: Porosity and Permeability	24
1. Determination of Porosity and Permeability	25
a. Low-frequency range	27
b. Near relaxation-frequency range	27
C. Sediment Shear Modulus	29
V. CONCLUSIONS	36
REFERENCES	37
APPENDIX A: Summary of Inverse Theory for Bottom Shear Modulus Profiles	45

LIST OF FIGURES

	<i>Page</i>
Figure 1. Fluid layer embedded between two different fluids with incident and transmitted sound wave	4
Figure 2. Typical shallow water experimental setup	7
Figure 3. Comparison of theoretical and experimental pressure field magnitudes and phases at 140 Hz, using forward model iteration	7
Figure 4. Comparison of theoretical and experimental pressure field magnitudes and phases at 220 Hz, using forward model iteration	8
Figure 5. Comparison of theoretical and experimental pressure field magnitudes at 140 Hz, using perturbative inverse technique	9
Figure 6. Geoacoustic models of the bottom	9
Figure 7. A plot of shot-generated time series and hodographs of the particle velocity for a 2-s time window	13
Figure 8. Measured phase velocity from continuous wave method and filtered pulse technique	14
Figure 9. The physical model	15
Figure 10. Boundary phase velocity as a function of frequency	16
Figure 11. Dispersion curves for elastic layer on a semi-infinite elastic substratum	17
Figure 12. Stacked time signals for vertical and horizontal particle velocities	19
Figure 13. Dispersion curves obtained by applying a multiple filter technique	20
Figure 14. Model environment used for generating synthetic seismograms	21
Figure 15. Propagation velocity V_{re} and anelasticity Q^{-1} values for coarse sand	26

Figure 16.	Propagation of a Ricker wavelet in silt, medium sand, and coarse sand	28
Figure 17.	The waterproof housing and various instruments that comprise the Bottom Shear Modulus Profiler.....	31
Figure 18.	Sensitivity- and frequency-corrected BSMP time series.....	32
Figure 19.	Frequency-corrected and time-averaged seismometer velocity and pressure power spectra	33
Figure 20.	Vertical and radial admittance data with associated coherences versus wave period	34
Figure 21.	Comparison of inverted shear modulus profile from experiment 121_5.....	35

I. INTRODUCTION

In a previous report,¹ the geoacoustic and geophysical properties of sediments were discussed in their relation to shallow water acoustics at low frequencies (20 to 500 kHz). The purpose of the present report is to review current methods of remote sensing and inversion of measurement data in shallow water to obtain these properties. We shall consider the acoustic spectrum in three different frequency regions: (a) ≥ 100 Hz, (b) 10–100 Hz, and (c) 1 to 10 Hz.

At frequencies ≥ 100 Hz, the reflectivity and scattering behavior of the seabed are used to determine its geoacoustic properties where the underlying sediment is assumed to be a viscoelastic fluid² rather than a simply lossless fluid. Hydrophones, spaced vertically and in range at planned locations, allow the processing of measurement data from either monochromatic cw or impulse sources to yield the required profiles. In this approximation, generation of shear waves is treated as an added loss to the compressional wave attenuation.

An important problem in shallow water acoustics is the determination of those geophysical properties of the seabed, sedimentary layers, and acoustic basement that account for the behavior of acoustic waves at frequencies below about 50 Hz. Although at these frequencies acoustic energy can penetrate deeply, there is usually little or no direct access to the geological structure for determining the actual geoacoustic properties. Remote sensing techniques must therefore be developed from which density profiles and compressional and shear wave profiles of velocity and attenuation can be inferred. Using this information, the acoustic wave equation can be solved.

In the frequency range below about 50 Hz, the poroviscous properties of the sediments must be treated using Biot theory. The consequences of Biot theory in this case have been studied by Stoll³ and Yamamoto,⁴ who have also applied inverse theory and methods to the problem. The two researchers are particularly interested in permeability, porosity, viscosity, and density. These quantities determine the poroviscous frequency number and the relaxation frequency below which the attenuation falls off approximately as the square of the frequency.

Below the acoustic cutoff of the shallow water sound channel, at approximately 1 to 10 Hz, energy is transmitted by interface waves along the bottom.⁵ Knowledge of Scholte and Rayleigh wave traces on the seabed allows the determination of the shear wave properties of the sedimentary and basement layers. Some previously developed seismic

techniques can also be employed for this purpose. The properties of the longer Rayleigh waves are used to determine the thickness of the sediment layer as well as the material properties of the acoustic basement. Furthermore, the dispersion of interface waves and the modal excitation of boundary and related shear waves, along with time signals stacked in range (synthetic seismograms), allow the determination of the seismoacoustic parameters of the sediment layer. These determinations are usually carried out by fast forward methods.

A forward method starts with a model of the scattering and transmission physics, usually in the form of acoustic pressure measurements and propagation loss runs versus range and depth. As model parameter values are varied, computer solutions are iterated until a best fit of model to data is obtained in some defined sense. Uniqueness and consistency of the final solution are not guaranteed. To rectify this, a theory of direct inversion has been developed that allows the treatment of uniqueness and optimal experimental design in the presence of interfering noise. Theoretically, with this technique one can use as a starting point the same model as in the forward case, though the experimental technique might require a different space and time configuration of measurement data.

The problem then becomes one of designing efficient experiments using sources whose properties are known with respect to frequency content, energy content, and the time domain signatures. If appropriate receivers are placed properly in range and depth, including bottom mounting, the data can be inverted to obtain the acoustic description of the sedimentary stratification and the underlying basement with some guarantee of uniqueness.

The problem of inverse experimental design and data analysis as applied to scattering experiments has had a long history in the solution of boundary value problems associated with the wave equations of quantum mechanics, nuclear physics, electromagnetics, seismology, and acoustics. The Appendix is a summary of inverse theory for the linear and nonlinear cases of shear modulus profiling adapted from Yamamoto and Torii.⁶ In this report, I review remote sensing methods and inversions presently used to find the acoustic properties of the bottom and subbottom as they affect shallow water propagation. However, I will consider only those cases where all three quantities – density, velocity, and attenuation – are determined or where geophysical parameters are measured that allow their determination. These geophysical parameters include permeability, the complex shear modulus, and porosity.

II. COMPRESSIONAL WAVE PROPERTIES

A. Introduction

Detailed reviews exist for the problem of remote sensing and inverse methods for compressional wave properties of shallow ocean sediments.⁷⁻¹¹ Here I outline only the major points.*

The basic remote sensing information required is the aperture- and band-limited values of reflected acoustic pressure waves as a function of depth in the water column. In deep water, the theoretical effort centers on a model of plane waves reflected by a one-dimensional inhomogeneous fluid layer.¹² In shallow water, the reflected plane wave is treated in modal form as the depth-dependent Green's function versus horizontal wave number.¹³

Compressional wave modeling in shallow water sediments usually assumes that the sediment is a horizontally layered viscoelastic fluid. Shear properties and Biot theory refinements are thus ignored for a first approximation. On this basis, both forward and direct inverse methods have been used to model the density and sound velocity profiles with depth. If the sediment attenuation coefficient is linear with frequency, then the attenuation profile can also be derived for this fluid medium model.

Forward methods, such as inferring bottom loss from propagation loss versus range experiments, have the disadvantage of possible incompleteness of model parameters. Direct inverse methods can test the uniqueness of models and can be used efficiently for designing appropriate experiments.

B. Inverse Methods

1. Plane Wave Reflection Coefficient versus Angle of Incidence

The plane wave reflection coefficient of the ocean bottom shows resonances both as a function of frequency and angle of incidence, depending on the properties of the ocean bottom. This is valid for any water depth since its input is the plane wave reflection coefficient of the bottom, which is independent of the water depth.^{7,8,11,12,14,15} However, there are practical limitations in shallow water.

*I have seen only one reasonably complete treatment of the actual inversion itself that started with at-sea measurements for compressional wave properties.⁷

Catholic University (CU) method of inversion

The CU method^{7,11,15} analyzes how the bottom reflection coefficient is affected by layer resonances that are carried by acoustic signals reflected from the ocean floor. The method exploits the fact that measured resonance parameters (locations, heights, and widths) are related to the layered-medium parameters (densities, layer thicknesses, and sound velocities of the layers) and hence provide a solution to the inverse problem. The model assumes a three-layer system — water, sediment, and basement. See Figure 1, where d is the sediment layer thickness, ρ is the density, c is the sound velocity, and θ is the angle of incidence.

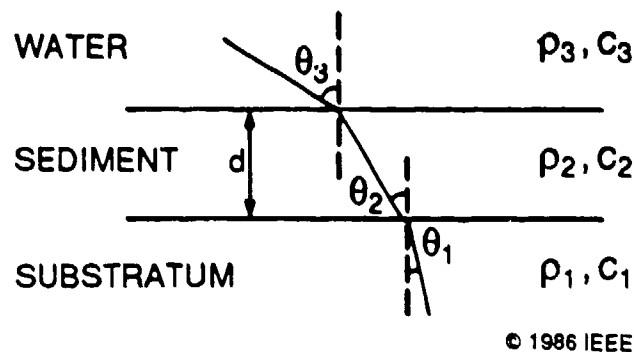


Figure 1. Fluid layer embedded between two different fluids with incident and transmitted sound wave (from Ref. 7).

If the square of the reflection coefficient is plotted on a three-dimensional graph versus the frequency (f) layer thickness product fd and incident angle θ_3 (from water to sediment angle), one gets a surface with a series of ridges and valleys. By plotting this upside down as the square of the transmission coefficient, we emphasize the sharp ridges descriptive of resonance-type processes. Nagl et al.^{7,11,15} proceed by interpreting the scattering process as a Breit-Wigner process of quantum physics for which the inverse solution already exists.

The experimentally measured resonance parameters are then related to the acoustic properties of the reflecting medium. By measuring the critical angle, the minimum value of the reflection coefficient, the spacing and width of the fd resonances at some angle, and the position and width of an angle resonance at a particular frequency, all the parameters describing the reflecting medium for a simple case — $c_1, c_2, \rho_1, \rho_2, d$ — can be deduced. Because the positions and widths of the angular resonances vary with angle,

it should be possible to determine a much larger set of medium parameters than for the simple case considered here. However, the method has not been exploited for either deep or shallow water.

D.J. Thomson¹⁴ has also investigated the problem of determining the material properties of the seabed, i.e., the density and sound speed profiles as a function of depth from an aperture- and band-limited knowledge of the acoustic reflection coefficient. He uses a direct inverse solution method from Candel et al.⁹ This method is based on the scattering of plane waves by a one-dimensional inhomogeneous medium. Thomson's use of the Born approximation provides him a high-frequency approximation, whereas the method of Candel et al. uses the low-frequency information to estimate the gradients for sound speed and density. Thomson presents an equation for the reflection coefficient that supports a noniterative method to deduce the admittance versus depth profile of an inhomogeneous medium from the impulse response. This equation is a nonlinear Fourier transform of the logarithmic derivative of the local admittance. Inversion of the integral transform enables the recovery of the admittance profile using the numerical integration of two first-order differential equations that require a single impulse response of the medium as reflection data. He concludes that reconstruction of both the density profile $\rho(z)$ and the sound velocity profile $c(z)$ should be no more difficult than determining one of these quantities. It is necessary to have reflection responses for two different probing directions, and four first-order differential equations have to be integrated instead of two.

Finally, Thomson points out that the derivation of the solution requires that the derivative of the logarithm of the vertical admittance in the vertical direction be independent of frequency. This requirement is satisfied for nonabsorbing media. It is also satisfied for absorbing media if the absorption depends linearly on frequency. There is evidence that this is not true for sediment absorption at the low frequencies below the relaxation frequency for sands and silts (see Section IV). Furthermore, the method does not apply to geoacoustic models that support multiple subbottom reflections.

2. Depth-Dependent Green's Function

The reflection coefficient can, in principle, be obtained from the depth-dependent Green's function. A method for inverting acoustic pressure measurements taken in shallow water using the depth-dependent Green's function has been developed by Rajan and his associates at the Woods Hole Oceanographic Institution (WHOI).^{7,10,13,16-18} The required input data are the magnitude and phase of the pressure field versus range with a monochromatic (cw) point source.

Synthetic aperture array data are obtained by towing a cw source away from moored receivers. The data are Hankel-transformed numerically to get the depth-dependent Green's function versus horizontal wave number. In terms of normal mode theory, the Green's function contains information about the nature of the discrete and continuous modal spectra and the plane-wave reflection coefficients of the waveguide boundaries. Specifically, the Green's function contains sharp peaks at horizontal wave numbers corresponding to the eigenvalues of trapped and virtual modes excited in the waveguide. The positions and magnitudes of these modal peaks can be sensitive to the acoustic properties of the bottom.

A geoacoustic model is then determined by matching the bottom model prediction of the depth-dependent Green's function to the experimental Green's function, particularly in the positions of the modal peaks. Forward model iterative techniques and perturbative inverse techniques have both been applied successfully to this inverse problem.

The WHOI method involves an exercise in which a cw source is towed at a fixed depth away from two moored receivers over an aperture that extends from zero range to several kilometers. The configuration is shown in Figure 2, where Z is depth. The receivers quadrature-demodulate the signal by beating the signal down to 0 Hz to remove the harmonic time dependence and then record the real and imaginary aspects of the spatial part of the acoustic pressure field $p(r)$.

The forward model iteration inversion consists of computing the theoretical Green's function for various values of the bottom parameters and finding in the positions and relative amplitudes of the modal peaks the parameter set that provides the best agreement with the experimental Green's function. Comparisons are also made between the measured and the theoretically computed pressure field magnitudes, so that a consistent, balanced fit is obtained in both domains.

For the perturbative inverse technique,^{13,17,18} the value of the location of the trapped-mode eigenvalues is the data used to invert for the difference $\Delta c(z)$ between the actual sound speed profile of the bottom $c(z)$ and that of a plausible reference model. Specifically, one locates the mode peaks and subtracts the mode peak locations to form Δk_n for each of the modes and then uses these as input to an integral equation for $\Delta c(z)$. The symbol k_n stands for the eigenvalues of the horizontal wavenumber k .

The equation for the Green's function is obtained as a straightforward application of first-order perturbation theory. It is readily extended to find attenuation and density profiles.^{13,17,18}

A demonstration of the technique starts with Figures 3 and 4, which show the pressure fields measured for a sandy bottom over a range-aperture of 1325 m in Nantucket Sound, Massachusetts, May 1984.

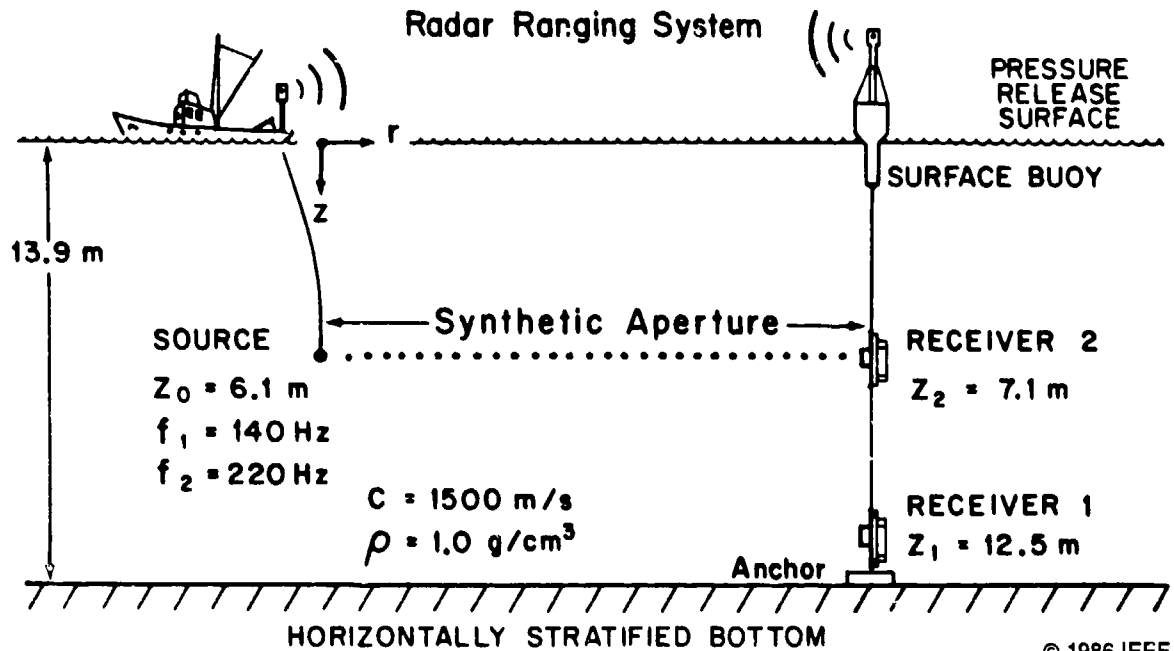


Figure 2. Typical shallow water experimental setup (from Ref. 7).

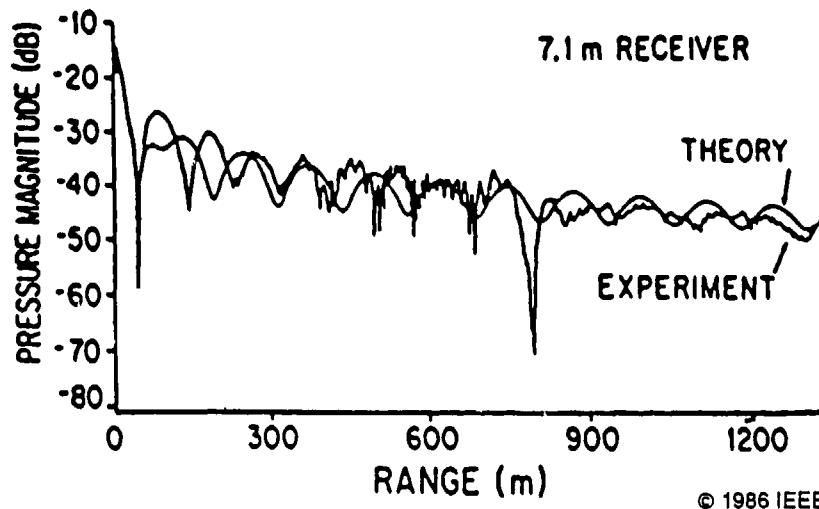


Figure 3. Comparison of theoretical and experimental pressure field magnitudes and phases at 140 Hz, using forward model iteration (from Ref. 7).

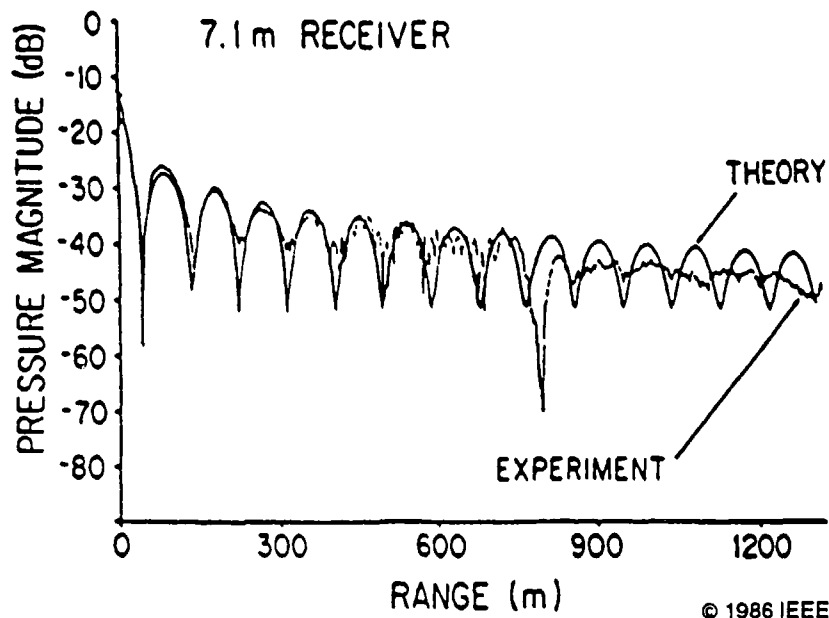


Figure 4. Comparison of theoretical and experimental pressure field magnitudes and phases at 220 Hz, using forward model iteration (from Ref. 7).

The magnitudes show strong spatial interference patterns. These patterns arise from the coherent combination of two normal modes of comparable strength at 220 Hz and one dominant and one weak mode at 140 Hz. The decay with range of the weaker mode at 140 Hz is also evident in the data. In addition, an increase of water depth from 13.9 to 14.6 m at a range of about 600 m has a pronounced effect on the 220 Hz modal cycle distance, which changes in that vicinity from about 125 to 150 m. The results of the forward model iteration inversion are shown in the theoretical curves for $p(r)$ in Figures 3 and 4. Excellent agreement is obtained for the 220 Hz data, but only fair agreement for the 140 Hz data. The likely reason for such a failure is probably the inherent simplicity of the bottom model, where only one or two parameters were varied at a time. A more general approach such as direct inverse theory is required. Here the bottom is not constrained to a few isovelocity or simple gradient layers.

In Figure 5, the pressure field generated by using the perturbative inverse scheme is shown for the 140 Hz data.

The agreement between theory and measured data is also excellent at 220 Hz, which is not shown. Note that this agreement was obtained after only three iterations of an inversion program that used a crude Pekeris model as a background. This demonstrates

the efficiency and robustness of the direct inverse approach as compared with standard forward modeling.

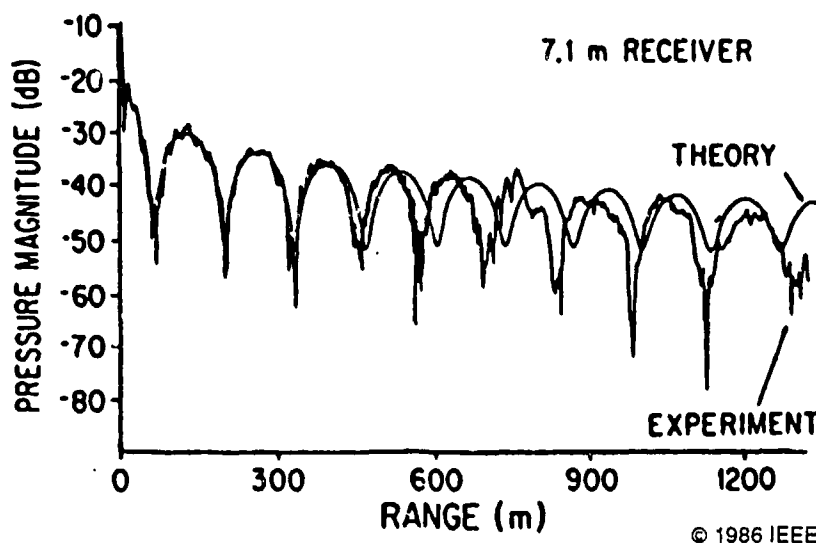


Figure 5. Comparison of theoretical and experimental pressure field magnitudes at 140 Hz, using perturbative inverse technique (from Ref. 7).

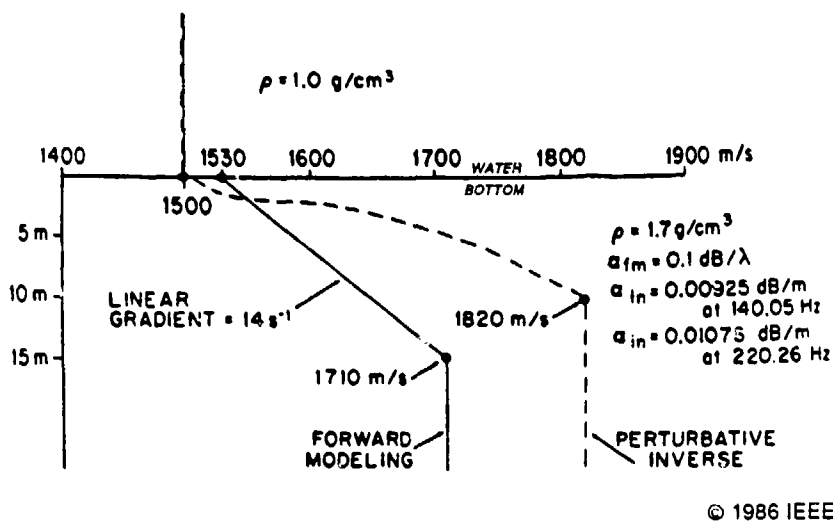


Figure 6. Geoacoustic models of the bottom produced by forward modeling and by perturbative inverse technique (from Ref. 7).

Figure 6 shows the geoacoustic models produced by the two techniques. The high near-surface sound velocity gradients produced by both models are consistent with Hamilton's results for sandy bottoms.¹⁹ The perturbative inverse technique also produces a continuously variable gradient profile until constrained at a sediment depth of

10 m. This allows the fit of data that cannot be handled by simpler models such as the constant gradient layer used in the forward approach. The symbol α in Figure 6 stands for attenuation.

Rajan reports²⁰ that the low-frequency inverse problem becomes linear as frequency is decreased and that linearization of high-frequency inverse problems can be obtained from this solution.

3. NORDA Method

The NORDA method^{7,21-23} involves two basic concepts in terms of the depth-dependent Green's function. First, the magnitude of the beam response of a horizontal array is approximately related to the magnitude of the depth-dependent Green's function. Specifically, the beam response will exhibit maxima at angles corresponding to the propagation angles of trapped and virtual modes. The angular resolution is in principle inversely proportional to the range aperture. In practice, it is still good for short array lengths and small numbers of receivers.

Second, the method uses the idea that for lossy bottoms the modal attenuation with range increases with mode number. This assumes that for bottom structures consisting of isovelocity layers with monotonically increasing velocity, the higher modes, with larger grazing angles, penetrate into the bottom more deeply and suffer greater attenuation. As a result, the source-receiver array offset is increased and the beam response is dominated by lower modes that interact with shallower portions of the bottom. Since a given mode with eigenangle θ_m can be viewed as being trapped by the reflecting horizon with lowest sound velocity c_m such that $c_m \geq c/\cos \theta_m$, the variable-offset beamformer response can be used to infer sound velocities in the bottom.

As the source-receiver offset is progressively increased, beamformed responses from deeply penetrating modes also progressively disappear owing to high in-situ absorption. Conversely, beamformed peaks corresponding to progressively shallower layers dominate the response in turn. Previous work²³ has shown that it is usually possible to identify compressional and shear wave velocity in a range of multilayered bottoms by moving the array farther away from the source and systematically isolating the critical angles of each layer.

III. SHEAR WAVE PROPERTIES*

A. Introduction

According to Akal and Jensen,²⁴ the excitation of shear waves in the bottom often becomes the dominant loss mechanism for waterborne sound in shallow water. These authors claim that a realistic model of the ocean bottom is a viscoelastic solid described by compressional and shear wave velocities, attenuations, and densities. Density and compressional wave speed can be found by direct methods, but shear wave properties are difficult to measure: their attenuation is high, and it is difficult to generate waves with predominantly transverse particle motions. However, the required parameters can be determined from measurements of interface waves on the ocean bottom. While shear properties of core samples can be measured in the lab, indirect determinations rely on the measurement of the boundary wave parameters of sediment-water, sediment-basement, and basement-water surfaces. There are three kinds of closely related interface waves: Rayleigh, Stoneley, and Scholte. Rayleigh waves propagate along the surface of a free solid. Stoneley waves are bound to the interface between two solids, i.e., sediment and acoustic basement. Scholte waves propagate along a liquid-solid interface.

Rauch⁵ has reviewed the role of interface waves in ocean seismoacoustics. He discusses the importance of the low velocity Scholte waves for seismic sensing of infrasound in coastal waters. Such waves are below waveguide cutoff. In seismics, the frequency 0.2 Hz separates short period tremors from medium and long period earth movements. For acoustic studies, 30 Hz divides infrasonics from sonics. In the following sections I concentrate on the problem of deducing the shear properties of sediments from interface waves.

B. Seismic Interface Waves

The usual method of exciting seismic interface waves in shallow water is to use broadband sources such as charges, airguns, water guns, and sledges. There are cw vibration exciters for individual frequencies and also for FM pulses. The usual receivers for interface waves are three-axis geophones mounted on the bottom along with a nearby hydrophone. This combination is called an ocean bottom seismometer (OBS). Because

*The figures in this chapter have been taken from different sources where symbols may have different, but clear, meanings.

the longer wavelengths of lower frequencies penetrate deeper, the depth-dependence of shear wave properties can be found by varying frequency. The low-frequency content of broadband signals is also used for this purpose.

The three types of interface waves have the following properties in common: (1) they are damped exponentially with distance from the interface in both directions, (2) their particle motion is elliptically polarized in the depth-range plane, (3) their velocity is closely related to the shear velocity of the solids involved, and (4) there is no low-frequency cutoff. Many acoustic measurements in shallow water have shown that infrasound is transmitted below the acoustic cutoff frequency of the water duct as Scholte interface waves.

Rauch and Schmalfeldt²⁵ have measured the characteristics of interface waves generated by 0.18-kg TNT shots at a range of 1 km in a water depth of 25 m. From an OBS they plotted sensor output versus time, including particle velocities from a three-axis geophone and the pressure output from the associated hydrophone (see plots in Figure 7, which also shows particle velocity hodographs). A pronounced long-lasting and low-frequency interface wavelet is seen to arrive much later than the high-frequency onset of the water wave. The recorded signals and hodographs show that the interface wave is detected only by the vertical and radial geophones. There is little or no energy in the transverse direction.

C. Dispersion of Interface Waves

Instead of using shots, Holt et al.²⁶ used a bottom-mounted vibration exciter as a cw source to generate interface waves at individual selected frequencies. They then determined the dispersion of Scholte- and Rayleigh-type waves and thereby deduced the shear modulus profile of the seafloor.

They studied the propagation characteristics of the cw pulses in detail. The received pulses had sound velocities in the range 100-200 m/s that are characteristic of Scholte waves. While Scholte waves could also be studied using hydrophones near the bottom, these are less sensitive to signals and more sensitive to ambient noise than geophones.

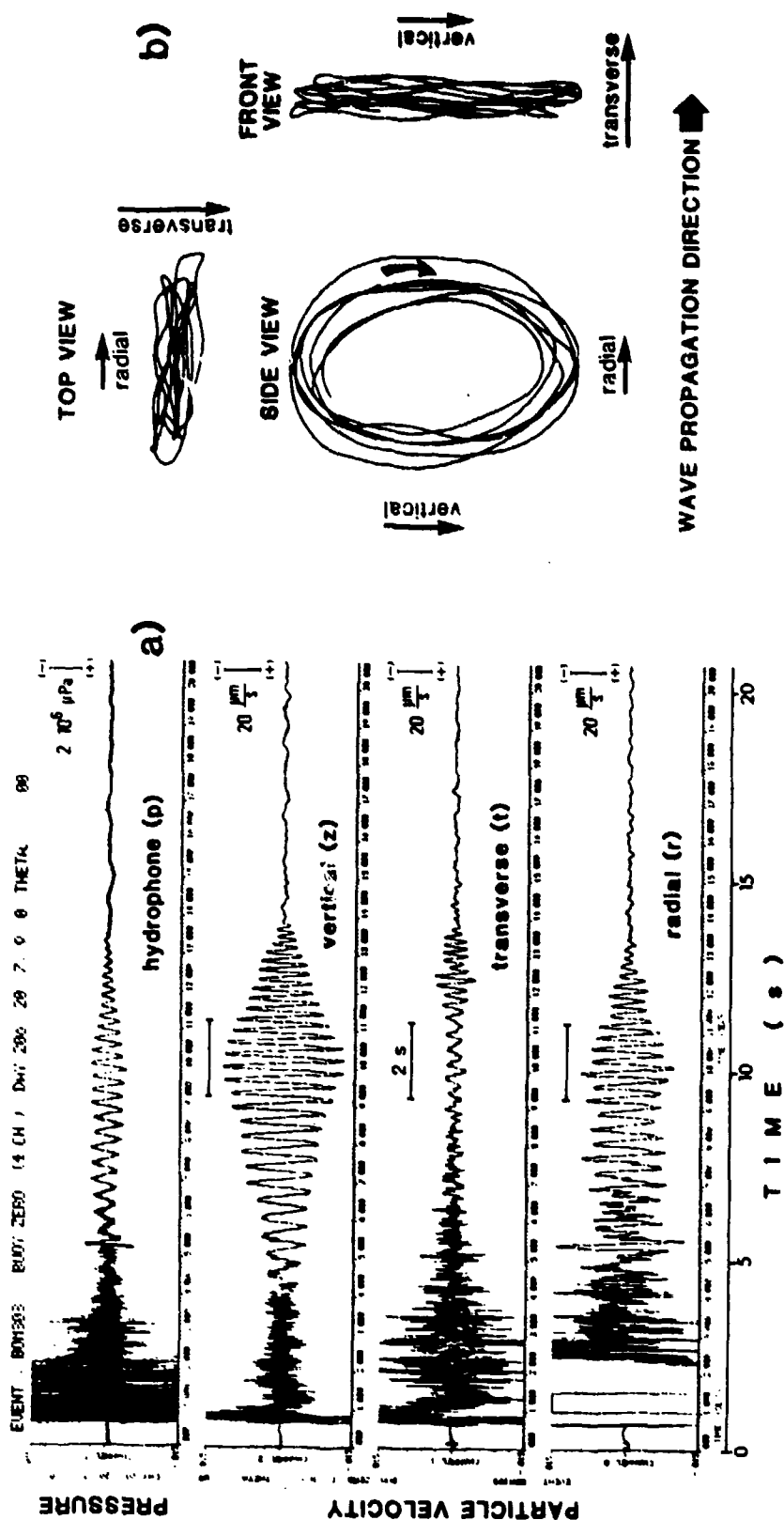


Figure 7. (a) A plot of shot-generated time series from three orthogonal geophones and one hydrophone. (b) Hodographs of the particle velocity for a 2-s time window (from Ref. 25). Details may be obtained from the authors. For our purposes, these should be understood as scaled amplitudes.

The authors first measured the phase velocity as a function of frequency between 5 Hz (limited by the vibrator) and 100 Hz (limited by the seismometers). They then found a best fit to the data as shown in Figure 8. With this best fit, they then calculated the group velocity using the standard formula

$$V_g(f) = \frac{V_p(f)}{1 - \frac{f}{V_p(f)} \frac{dV_p(f)}{df}} \quad (1)$$

where f is the frequency in hertz, V_p is the phase velocity in meters per second, and V_g is the group velocity in meters per second.

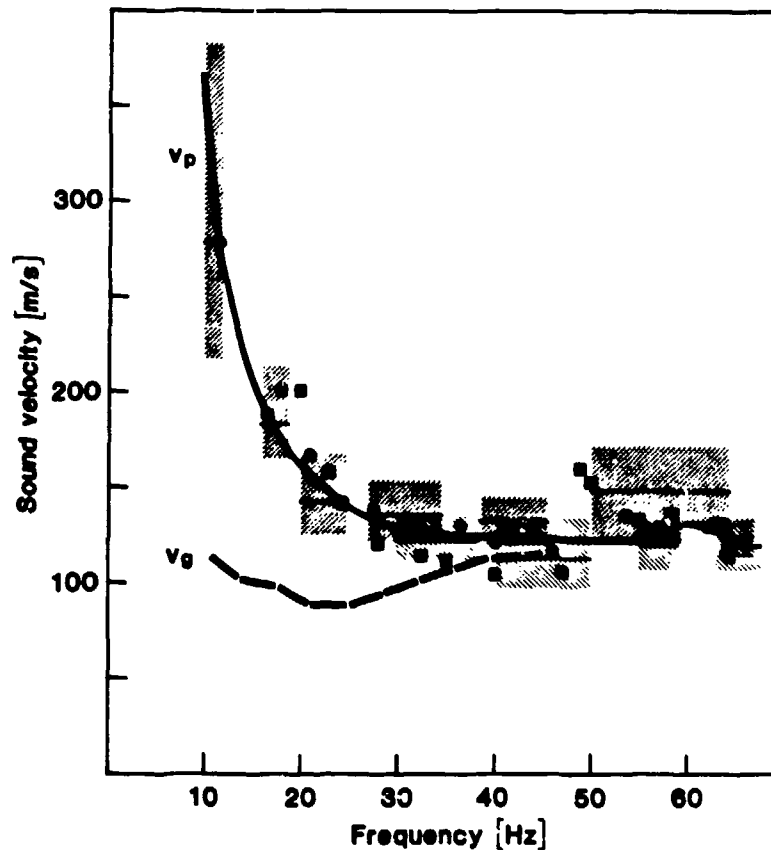


Figure 8. Measured phase velocity from continuous wave method (■) and filtered pulse technique. (Hatched areas: width given by the bandwidth of the filter; height given by the phase variations across the pulse. Average values are denoted by horizontal lines.) (●) denotes measured phase velocity at certain given frequencies in the pulses. The group velocity (broken line) is calculated from the fully drawn phase velocity curve (best fit) (from Ref. 26).

The inverse problem is to find the shear velocity of the sediment layer as a function of depth using the geoacoustic model of Figure 9. The water column and solid substrate are homogeneous and semi-infinite, but the density and elastic parameters of the sediment can vary arbitrarily with depth. The depth-separated wave equation of the inhomogeneous sediment layer is solved by numerical integration.²⁷

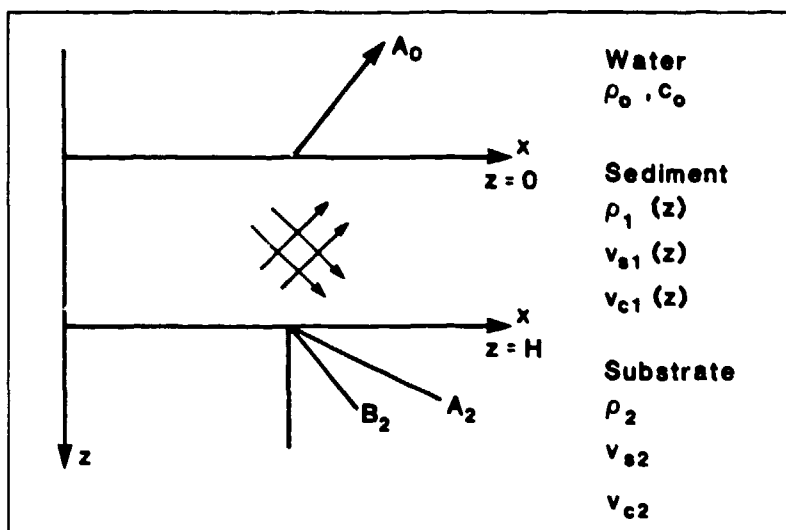


Figure 9. The physical model (from Ref. 26).

Holt et al. solved the wave system for the model shown in Figure 9 as follows. If A_0 is the upgoing compressional wave in the water and there are two downgoing waves in the solid substrate A_2 (a compressional wave) and B_2 (a shear wave), then setting boundary conditions at the two sediment interfaces allows the determination of the dispersion equation.²⁸ The boundary conditions require that the stress-displacement vector is continuous at the interfaces. In Figure 9, ρ is the density, v_s is the shear wave velocity, v_c is the compressional wave velocity, c_0 is the sound speed in water, and z is depth.

Using this theoretical model, the sediment parameters are varied and the problem is solved repeatedly in the forward manner until a best fit to the experiment data is obtained. Figure 10 summarizes the optimum parameters for the model to give the solution shown for the phase velocity. In this case, the best fit is obtained for a sediment

thickness of $H = 4.5$ m and a sediment shear velocity v_{S1} , which increases linearly with depth z as

$$v_{S1} = 135 + 15 \cdot z . \quad (2)$$

The most important parameters are layer thickness and the mean shear velocity in the layer.

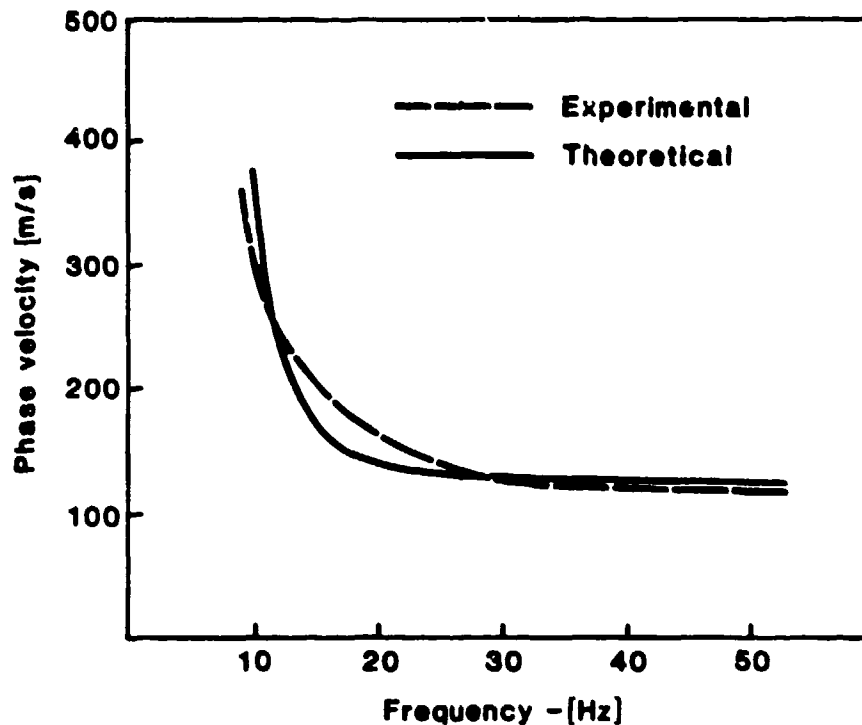


Figure 10. Boundary phase velocity as a function of frequency. Theoretical results calculated with $H = 4.5$ m, $v_{S2} = 135 + 15 \times z$, $\rho_1/\rho_0 = 2$ and $\rho_2/\rho_0 = 3$, $v_{S2} = 800$ m/s, $v_{c1} = v_{c2} = 2000$ m/s (from Ref. 26).

D. Sediment Shear Properties

Jensen and Schmidt²⁹ give simple formulas that relate the speed and attenuation of interface waves to those of body shear waves. They use seismic records to find the shear speed and attenuation profiles in the upper sediment layers.

For two homogeneous media in contact, the Scholte wave is nondispersive. Its propagation speed, V_{sch} , and attenuation, Δ_{sch} , are

$$V_{sch} = 0.9V_s \quad (3)$$

and

$$\Delta_{sch} = 1.1 \Delta_s, \quad (4)$$

where V_s is the shear velocity and Δ_s is the shear attenuation in decibels per unit length.

These formulas are accurate to within a few percent for unconsolidated sediments (clay, silt, and sand) with low shear speeds. Scholte wave properties are independent of densities and compressional wave properties in the two media.³⁰

When sediment is layered, Scholte waves become dispersive, and finite-ducted shear modes appear. Figure 11 shows dispersion curves for a sediment layer of low shear speed β_2 and thickness H of a high-shear-speed solid acoustic basement or substrate.³¹ The M 's stand for the mode numbers. The lowest mode, M_0 , is an interface wave that in

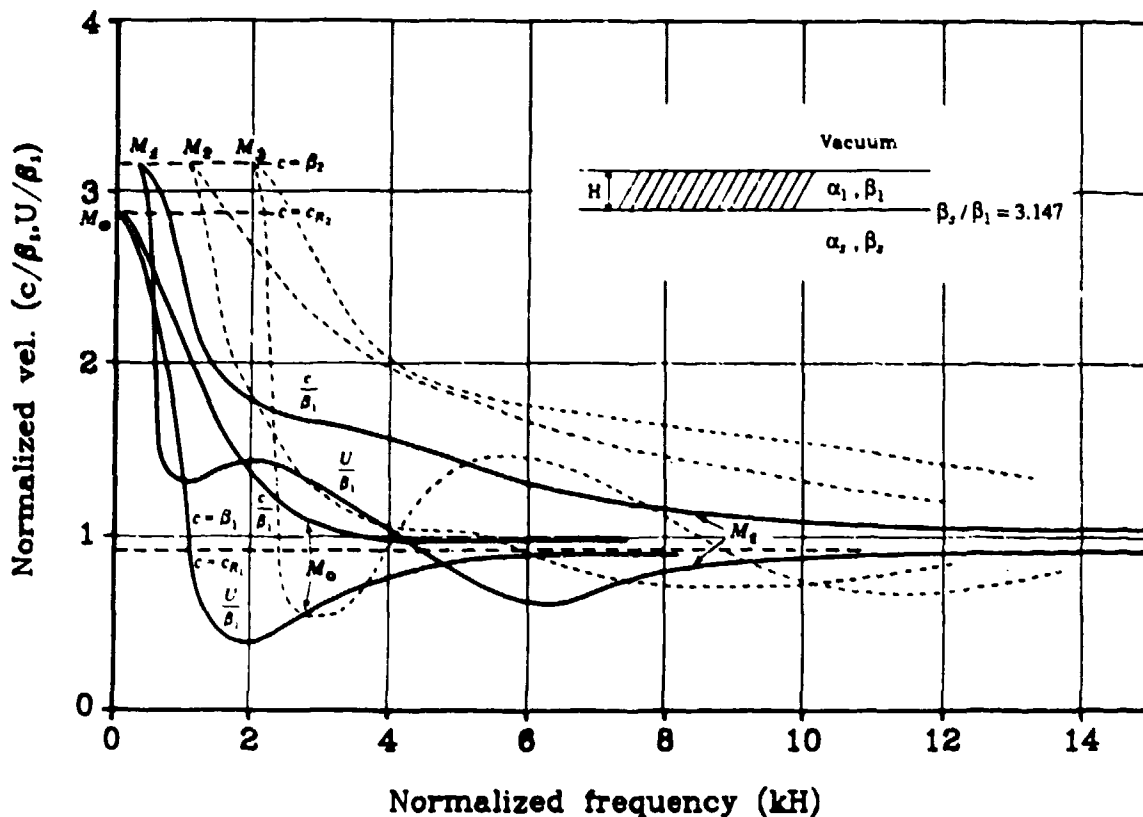


Figure 11. Dispersion curves for elastic layer on a semi-infinite elastic substratum (from Ref. 29).

the low-frequency limit $kH \rightarrow 0$ propagates as a Rayleigh wave on the substrate. In the high-frequency limit $kH \rightarrow \infty$ the lowest mode propagates as a Rayleigh wave on the surface of the upper layer. The surface waves all have a cutoff frequency at which they propagate with the shear speed of the substrate. In the high-frequency limit these modes propagate with the shear speed of the upper layer. There is no Stoneley wave because this requires a change in shear speed of $<10\%$ across a solid-solid boundary.

Information about bottom shear properties is usually obtained from measured dispersion curves. If experiments show negligible dispersion, the sediment is homogeneous to a depth of one or two wavelengths, which is the penetration depth of the Scholte wave. Equations 3 and 4 can then be used to determine the shear properties of the sediment.

Previous measurements on Scholte waves over sand or silt, between 3 and 35 Hz, have shown a variation of attenuation greater than two or more orders of magnitude, from about 0.02 to 2.3 dB/ λ_s .²⁹ Here λ_s stands for the shear wavelength. Very low attenuation values go with low frequencies (3 to 5 Hz). Two possible explanations for this large variation are: (1) shear attenuation decreases with depth and low-frequency Scholte waves penetrate deeper, and (2) attenuation varies with a power of frequency between 1 and 2. The Biot model predicts such a dependence.³²

Two types of measurements can be used to determine shear speed and shear attenuation profiles: (1) Stacked time signals for both vertical and horizontal particle velocities are shown in Figure 12 as recorded by a geophone on the ocean bottom. The sources were explosive charges detonated near the seafloor in 20 m of water. The dispersed low-frequency Scholte waves are seen to arrive with group velocities between 78 and 235 m/s. (2) By using a multiple filter technique³³ on the recorded times series at a fixed range of 1.7 km, dispersion diagrams are obtained as shown in Figure 13. The contours indicate relative energy levels. Note that there is more information in the propagation of the horizontal radial component of the particle velocities. Figure 13 shows that the energy arrives in three discrete modes of which the slowest arrival is the Scholte mode (M_0) with energy centered at about 2 Hz. The first shear mode (M_1) is strongly excited with maximum energy around 2.8 Hz, while the second shear mode (M_2) is weak.

The measurements are then applied to a numerical model outlined in the next section in a trial-and-error fashion to arrive at computed dispersion characteristics that agree with the measurements of Figures 12 and 13. The compressional wave properties

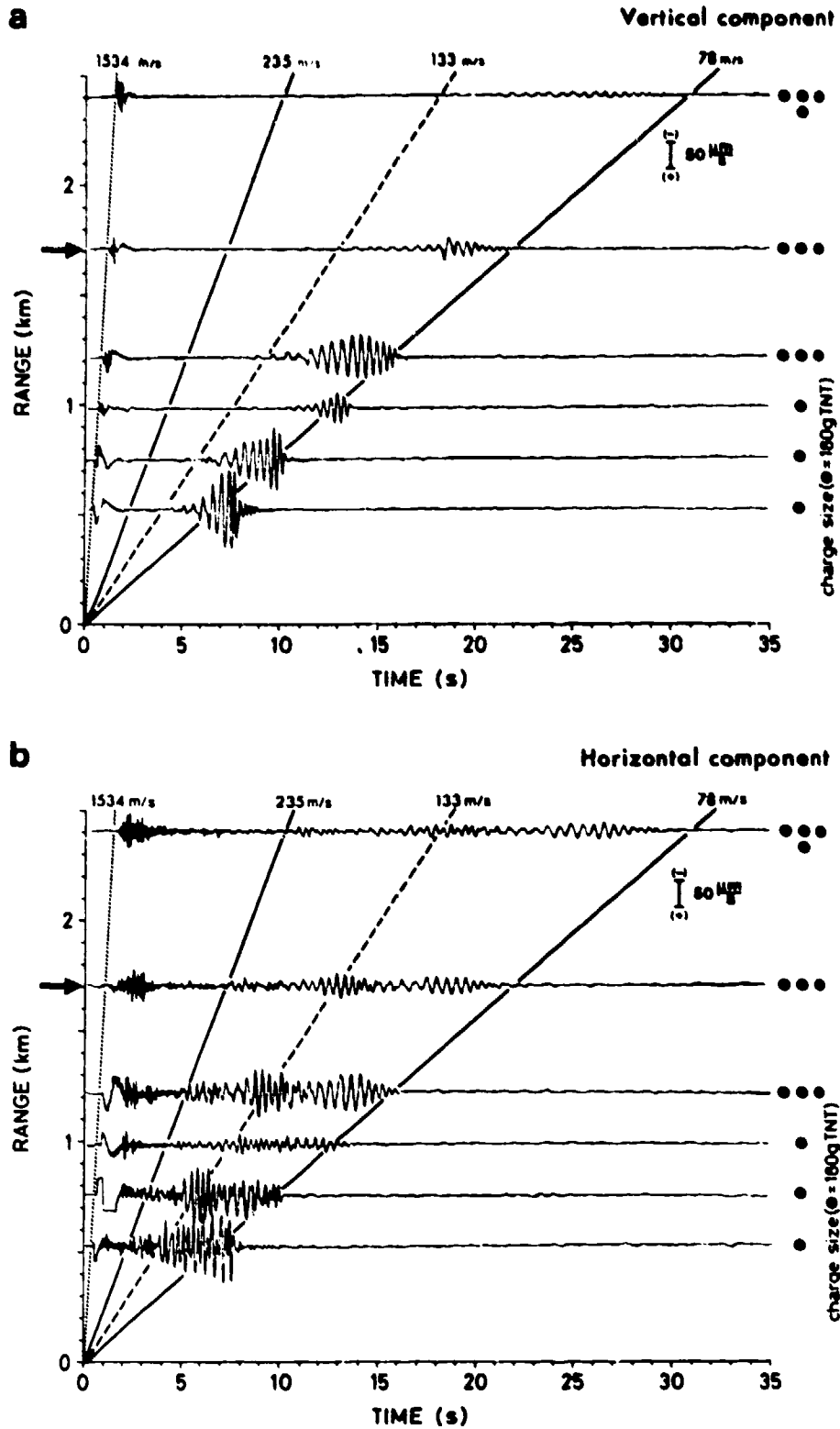


Figure 12. Stacked time signals for vertical (a) and horizontal (b) particle velocities as recorded by a geophone on the seafloor (from Ref. 29). A ● represents one charge unit.

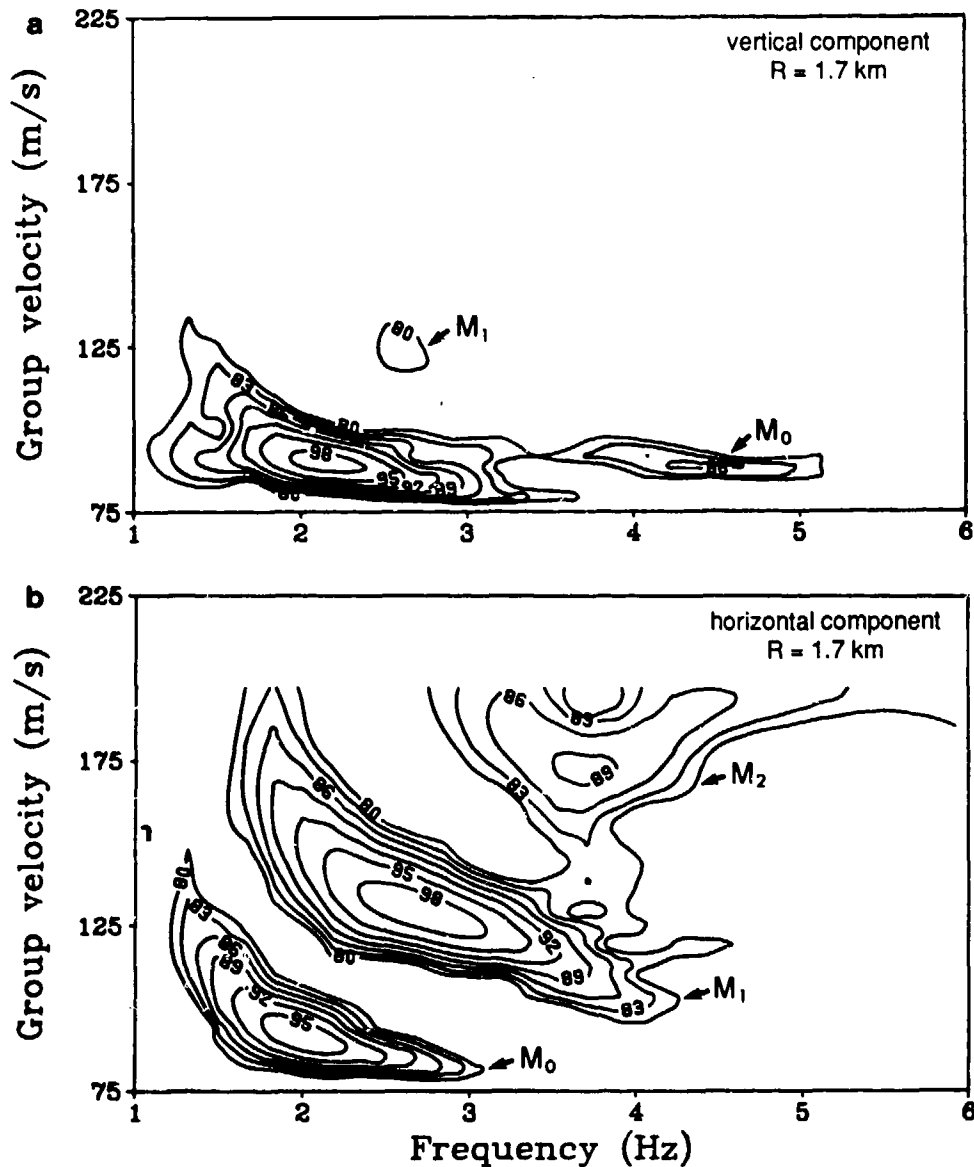


Figure 13. Dispersion curves obtained by applying a multiple filter technique to the experimental records at range $R = 1.7$ km. Energy is seen to be propagating in three discrete modes: M_0 , M_1 , and M_2 (from Ref. 29).

and densities are fixed a priori for the unconsolidated sediment since they are known to have a negligible effect on the propagation of interface waves. Figure 14 shows the final choices of the shear speed profile C_s and shear attenuation profile β_s , with the assumed compressional wave properties C_c and β_c and density ρ . In this figure, β_s and β_c stand for shear and compressional wave attenuation, respectively.

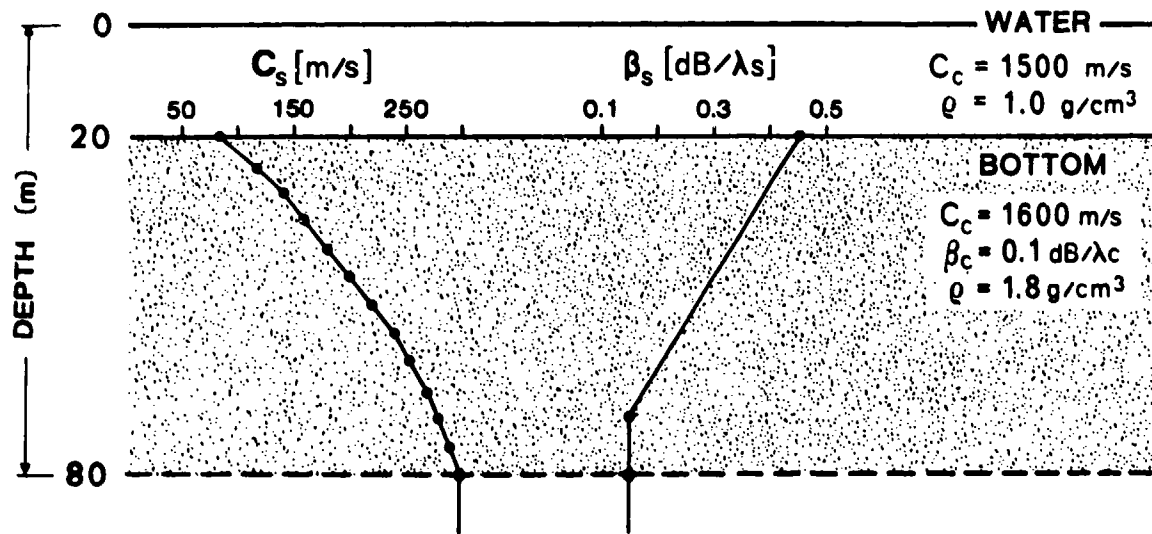


Figure 14. Model environment used for generating synthetic seismograms (from Ref. 29).

E. Schmidt's Numerical Method

Schmidt^{34,35} has developed a fast numerical method to evaluate viscoelastic physical models of the seabed as a propagating medium for seismic waves. He analyzes the excitation and propagation of interface waves, obtaining many of the basic features observed during experiments conducted by the SACLANT ASW Research Centre.

One of the purposes of investigating interface waves is to determine seabed properties that cannot be measured directly. A distinct transition frequency exists below which the propagation of the first interface wave is a Rayleigh wave on a pure acoustic basement half-space. Its velocity and damping yield information on the properties of the basement. The transition frequency is the first thickness-shear frequency of the sediment layer as an infinite plate and is a direct measure of the sediment shear velocity. Above the transition frequency, the first interface mode measures the properties of the water-sediment interface, and its properties determine the properties of the sediment layer. The second interface mode above the transition frequency is related to the sediment-basement interface and contains coupled information on both media. If there is more than one sediment layer, several interface modes will appear; their interpretation can be complex.

The data-fitted theoretical model is then used to compute dispersion curves and modal energy content with a prescribed frequency dependence of shear attenuation. This dependence turns out to be quadratic. For an unconsolidated sand-silt bottom, the shear

velocity is found to increase with depth from 85 m/s at the seafloor to 300 m/s at 60 m depth. The shear velocity increases with depth at the rate 3.58 m/s/m. The shear attenuation at 3 Hz decreases with depth from 0.45 dB/ λ at the seafloor to 0.15 dB/ λ at 60 m depth.

Schmidt's technique³⁵ is similar to those described by Kutschale³⁶ and DiNapoli and Deavenport,³⁷ who take a Green's function approach based on the Thomson-Haskell matrix method. However, Schmidt's method is computationally more efficient.

The environment is approximated by a series of horizontally homogeneous and isotropic elastic continua with Lamé constants λ and μ and density ρ . The displacement and stress components are expressed in terms of three scalar potentials, each of which must satisfy a wave equation. After the Hankel transform is applied, the boundary conditions at each interface yield a linear system of equations in the Hankel transforms of the potentials. All displacement and stress components can then be expressed as Hankel transform integrals with transforms of the potentials included in the kernels.

There are two parts to the numerical evaluation. First, the Hankel transforms of the potentials are found at discrete horizontal wave numbers. The equations are then solved conveniently by Gaussian elimination. Then, the desired displacement and stress components are evaluated at a given depth and range with the fast-field integration technique.^{36,37}

Schmidt applies his method to a set of seven test cases with different sediment materials (silt and sand) and thicknesses (5, 30, 50 m) and two different substrates (limestone and basalt). He also studies the effect of a linear gradient by using stepped layers. The water depth is 100 m in all cases with a source amplitude of 1 Pa re 1 m at 50 m depth.³⁵

He uses mode transition zones from the theory of plate vibrations, where they appear as thickness-shear frequencies for an infinite elastic plate performing free shear vibrations with vanishing vertical displacements at the edges. For a silt layer, the first thickness-shear frequency f_{TS} would correspond to that of a free silt plate of double the actual thickness

$$f_{TS} = C_T / (4d_s), \quad (5)$$

where C_T is the shear velocity and d_s is the thickness of the layer. If the parameters of silt are applied to Eq. 5, then we get $f_{TS} = 1$ Hz (i.e., $C_T = 200$ m/s) and $d_s = 50$ m. Thus

$$f_{TS} = 200/200 = 1 \text{ Hz} .$$

Because the transition frequency can be observed experimentally,²⁵ its correlation with the thickness-shear frequency can be used to determine the shear wave velocity in a single sediment layer overlying a rigid half-space.

In general, direct measurements of shear properties are difficult to perform. However, both shear wave speed and attenuation profiles can be inferred from measured dispersion characteristics of bottom interface waves. The propagation of Scholte waves depends on sediment shear properties. Sediment shear wave speeds are about 85 to 300 m/s with shear wave attenuations of 0.15 to 0.45 dB/ λ at 3 Hz. In the next section, I consider the remote sensing of the Biot geophysical properties of shear modulus, permeability, and porosity, which allow the determination of the geoacoustic properties from Biot theory.

IV. BIOT GEOPHYSICAL PARAMETERS

A. Introduction

Yamamoto and his associates at the University of Miami are concentrating on a program of remote sensing and inversion of bottom seismic data to determine the Biot geophysical properties of marine sediments. They are particularly interested in obtaining depth profiles of porosity and permeability from synthetic seismograms³⁸ and complex shear modulus profiles in the sediments as a function of depth using ocean wave excitation of the bottom.^{6,39} Geoacoustic properties can be derived from these parameters. This unique program is discussed here.

B. Synthetic Seismograms: Porosity and Permeability

Plane wave reflection and transmission coefficients play an important role in the calculation of synthetic seismograms and the interpretation of acoustic data.

Claerbout⁴⁰ showed how to synthesize a layered medium from its acoustic transmission response. He presented a direct (noniterative) inverse method of determining an acoustic layered medium from the seismogram caused by a time-limited plane wave incident from the lower half-space of Claerbout's model. He showed that one side of the autocorrelation of the seismogram that results from an impulsive source at depth is the same as the seismogram from an impulsive source on the surface. This transforms the problem to the acoustic reflections problem solved by Kunetz.⁴¹ Both the deep-source time function and the layering can be determined from a surface seismogram.

Goupillaud⁴² solved the inverse problem of determining the medium from the seismogram. Kunetz showed that the inversion should be stable and will be so if the observed reflection seismogram is one side of an autocorrelation. His correlation function is the autocorrelation of the seismogram observed from an impulsive source emerging from depth. Thus the impulsive transmission problem is transformed to Kunetz's reflection problem by an autocorrelation.

Previously, most synthetic seismograms were calculated for rigid elastic models that ignored the effects of dispersion and attenuation. In a more realistic model of marine sediments in which the elastic material is replaced by viscoelastic or porous viscoelastic material, the response at an interface between two different layers is more complicated. Reflection and transmission coefficients are complex numbers for a viscoelastic model.

Furthermore, Deresiewicz and Levy have shown that there is mode conversion between fast and slow compressional waves and generation of shear waves at the interfaces of a layered porous viscoelastic medium.⁴³

Ganley⁴⁴ outlined a method that allows the calculation of one-dimensional theoretical seismograms and includes the effects of absorption and dispersion. The parameters that are specified for the model are layer thicknesses and density, phase velocity, and the specific attenuation factor (Q) in each layer. It is also necessary to have equations defining the absorption and dispersion relations. Futterman⁴⁵ derived a Kramers-Kronig relation that allowed the calculation of dispersion for a given absorption function. Ganley used one of Futterman's absorption-dispersion pairs to compute examples at the surface as well as at several depths for a simple test model.

In Ganley's model, the attenuation is accounted for mathematically by allowing the elastic modulus to be a complex function of frequency (viscoelastic model). This results in a complex velocity and wave number; the reflection and transmission coefficients also become complex functions of frequency. The attenuation model is applicable to plane waves in a flat, layered model.

Turgut and Yamamoto³⁸ use a more realistic Biot model of marine sediments than Ganley in which the viscoelastic material is replaced by a porous viscoelastic material for which the response at an interface between two different layers is more complicated. In this latter case, Biot theory predicts mode conversion^{46,47} between fast and slow compressional waves at interfaces. Their model includes this mode conversion as an energy loss mechanism. This type of energy loss is even more important when multiple reflections occur within layers. They present a possible method of predicting porosity and permeability of marine sediments by using information on the frequency dependence of the phase velocity and attenuation of the fast compressional waves. Biot theory enables the determination of porosity and permeability of marine sediments once the frequency-dependent velocity and anelasticity (Q^{-1}) are measured.

1. Determination of Porosity and Permeability

The propagation of acoustic waves through marine sediments can be considered as a fluid-solid (inertial and viscous) coupling problem governed by hydrodynamic properties of sediment, porosity, and permeability. The inertial coupling is governed by porosity; the viscous coupling by permeability. Jackson and Anderson point out that a viscous coupling is a relaxation process.⁴⁸ Therefore, the velocity V and anelasticity Q^{-1} for the fast compressional wave are frequency-dependent. Turgut and Yamamoto calculate the

compressional wave velocity and anelasticity from the Biot-Stoll equation using the permeability k_s , porosity β , shear modulus G , and frame loss coefficient δ of coarse sand. Figure 15 shows that the anelasticity becomes maximum at about 32 Hz for coarse sand. This peak frequency is the relaxation frequency of the sand. The relaxation frequency of a saturated sediment is given by Yamamoto⁴⁴ as

$$f_r = 0.1 \frac{\beta v}{k_s}, \quad (6)$$

where v is the kinematic viscosity of pore fluid.

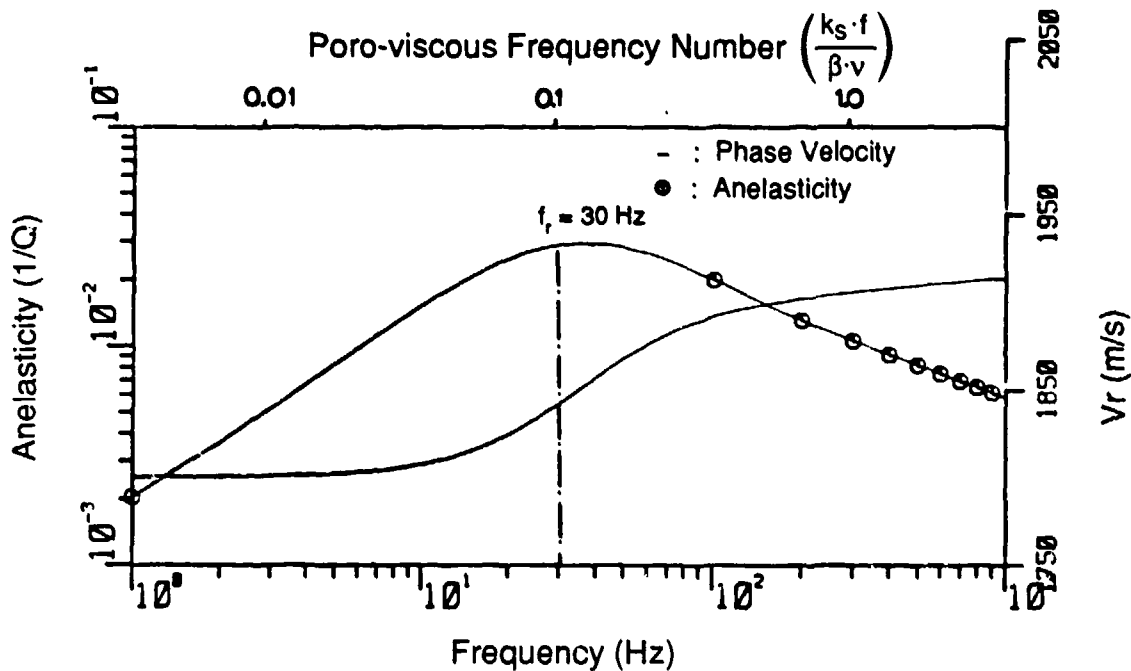


Figure 15. Propagation velocity V_{re} and anelasticity Q^{-1} values for coarse sand (from Ref. 38).

The weak frame ($K_r, K_f \gg K_b, \mu$) approximations in Plona and Johnson⁴⁹ are valid for most marine sediments. K_r is the bulk modulus of the grains, K_f is the bulk modulus of the fluid, K_b is the bulk modulus of the frame, and μ is the shear modulus of the frame. Thus, we can use the following approximate relations in their respective frequency bands.

a. Low-frequency range

$$V = V_o = \left(\frac{K_f/\beta + G'}{\rho} \right)^{1/2}$$

and

$$Q^{-1} = 2\pi \frac{(\rho - \rho_f)^2}{\rho \rho_f} \frac{k_s}{v} f + \delta', \quad (7)$$

where V is the compressional wave velocity and subscript o stands for low-frequency limit.

$$\delta' = \frac{\delta G'}{\rho V_o^2},$$

where δ is the skeletal frame loss, and

$$G' = G \left(2 + \frac{2n}{1-n} \right).$$

Here n is the Poisson ratio and G is the shear modulus.

b. Near relaxation-frequency range

$$Q^{-1} = Q_{\max}^{-1} = \frac{1}{3} \beta \frac{(\rho - \rho_f)^2}{\rho \rho_f} + \delta'. \quad (8)$$

If we measure V and Q^{-1} of a sediment as a function of frequency, we can determine the porosity and permeability from equations 7 and 8. In addition, the frame loss δ can be determined if the shear modulus G is known.

Figure 16 from Reference 38 shows synthetic seismograms calculated for a Ricker wavelet propagating through homogeneous layers of (a) silt, (b) medium sand, and (c) coarse sand. A Ricker wavelet has the spectrum

$$N(\omega) = \omega^2 \exp(-\omega^2/\omega_o^2), \quad (9)$$

where ω is the angular frequency and ω_o is the peak angular frequency.

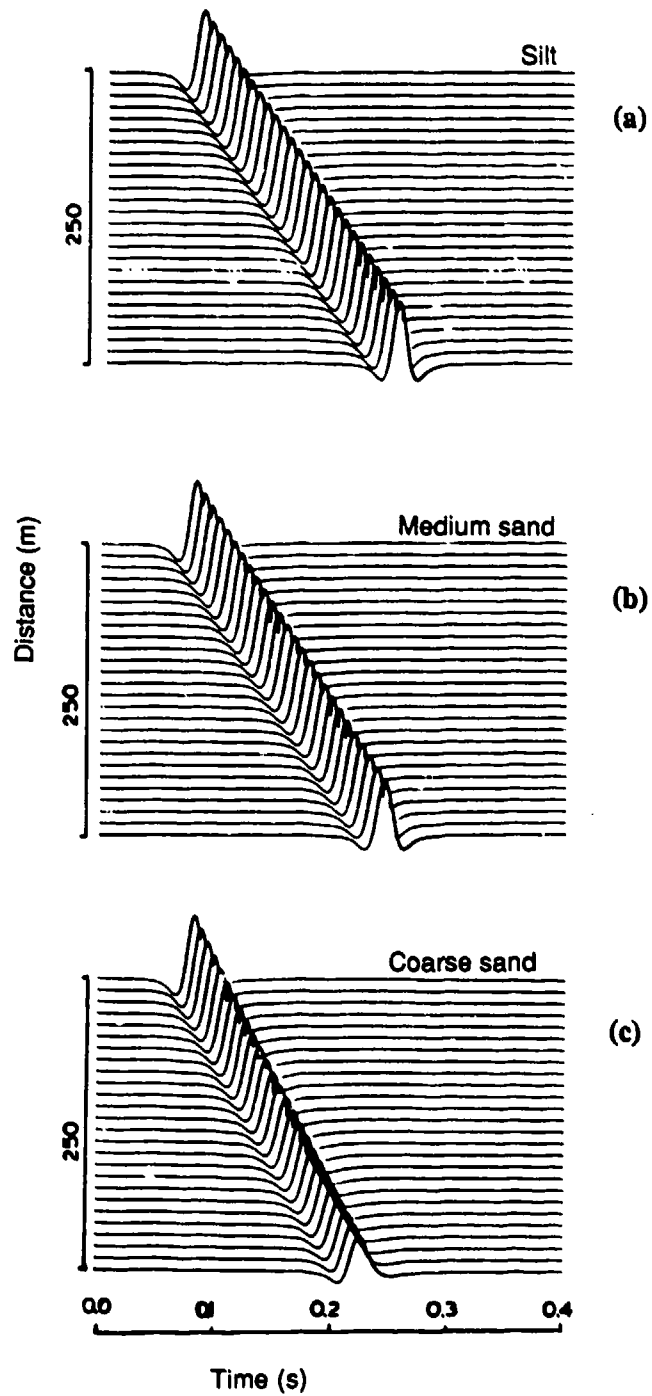


Figure 16. Propagation of a Ricker wavelet in (a) silt, (b) medium sand, and (c) coarse sand (from Ref. 38).

C. Sediment Shear Modulus

Yamamoto and Torii⁶ have developed a theory that enables seabed shear modulus profiles to be extracted by inverting measurements of seabed motion and pressures induced by water waves at one point.

As surface water waves propagate through intermediate to shallow water, they induce motions of the seabed sediments through variations in pressure on the seafloor. According to models developed by Yamamoto and others, the layered seabed sediments can be seen to behave in a massless, incompressible, elastic manner in response to pressures induced by water waves.⁵⁰⁻⁵² Under these circumstances one can predict realistically the seabed response to passing water waves if the sediment shear modulus is known at every depth.⁵³ Conversely, through the use of geophysical inverse methods, one can extract the profile of the shear modulus as a function of depth from measurements of seabed motion and pressure induced by water waves.

Linear inverse theory is used combined with Yamamoto's theory of wave-seabed interaction (see Appendix A). The uniqueness and consistency of the inversion was established by numerical tests using synthetic data without noise. As a practical test on noisy data it was shown that good agreement was obtained between the inverted shear modulus profile and direct measurements at the Mississippi River Delta. Theoretical assumptions of small amplitudes and elastic sediment behavior were validated by examining time series of seabed displacement, dynamic phase spectra, and profiles of seabed shear strain.

Based on the success of these experiments, a Bottom Shear Modulus Profiler (BSMP) was developed.⁵⁴ Comparisons of BSMP inversion results, in situ sediment strength tests, and laboratory analysis of core samples show that this technique can accurately measure the magnitude and depth structure of the sediment shear modulus. The shear modulus of a marine sediment is one of the more important parameters for many theories modeling seismic, acoustic, and surface gravity wave propagation in the ocean. Existing, accepted methods of measuring a profile of the sediment shear modulus, such as making standard penetration boreholes or measuring the travel time of cross-hole shear waves, are cumbersome and slow. Such methods also suffer from the unavoidable problem that the act of boring, drilling, or removing the sediment disturbs the sediment framework and grain structure. This can seriously affect the sediment shear modulus, especially for cohesive muds and clays. In contrast, this new BSMP system is fast and unobtrusive to the seabed. It seems possible that the BSMP could also become a standard tool for engineering surveys of marine sediments.

Additional experiments were conducted off the New Jersey coast in August 1986.^{54,55} Of concern was the fact that the accurate measurement of the small seabed motions occurring in a typical marine environment is not a trivial problem. The typical seabed displacement amplitude caused by a moderate sea on a sandy bottom is of the order of a millimeter. A further problem is the extremely low frequency of surface gravity water waves, which are typically in the range of 0.06 to 0.3 Hz (periods of 17 to 3 seconds). The motion sensors need to be firmly coupled to the seabed, allowing no slippage or relative motion between the sediments and the instruments. This seabed-to-instrument coupling is a difficult quantity to assess and may be a significant problem on softer, more slippery muds and clays. Also, the instrumentation package as a whole needs to be waterproof and pressure-resistant to depths of 200 m or more. Figure 17 shows a detailed diagram of the major components of the BSMP instrumentation package. The main body of the instrument housing, the seismometer supports, and the bottom base plate are made of aluminum alloy. The hemispherical glass cap is designed to withstand a depth of 600 m and to have a low profile in order to minimize horizontal hydrodynamic forces on the unit. In use, a slight vacuum is applied inside the glass hemisphere to hold the cap in place and reduce leakage by compressing the "O" rings. Fully assembled, the entire BSMP unit has a mass of about 45 kg.

The heart of the BSMP sensor is formed of three seismometers mounted in one vertical and two perpendicular horizontal directions. Each seismometer measures motions along its principal axis only, and the three directions are labeled vertical, horizontal, and transverse. A compass and pendulum tiltmeter are included in each BSMP unit to determine the orientation of the seismometers. The sensitivity of the seismometers is 45 volts/m/s with a resolution threshold of 3×10^{-8} m/s.

Figure 18 shows the sensitivity and frequency-corrected BSMP time-series for the four measured quantities required for the inversion process. Figure 19 shows the velocity and pressure power spectra indicating the ocean wave (swell) periods contributing energy for this technique. In Figure 20, the important parameters, admittance and coherence, are plotted for one experiment. Figure 21 provides a comparison of the shear modulus inversion, reference data from a sediment shear strength borehole, and laboratory analysis of a vibracore sample. The agreement is remarkable.

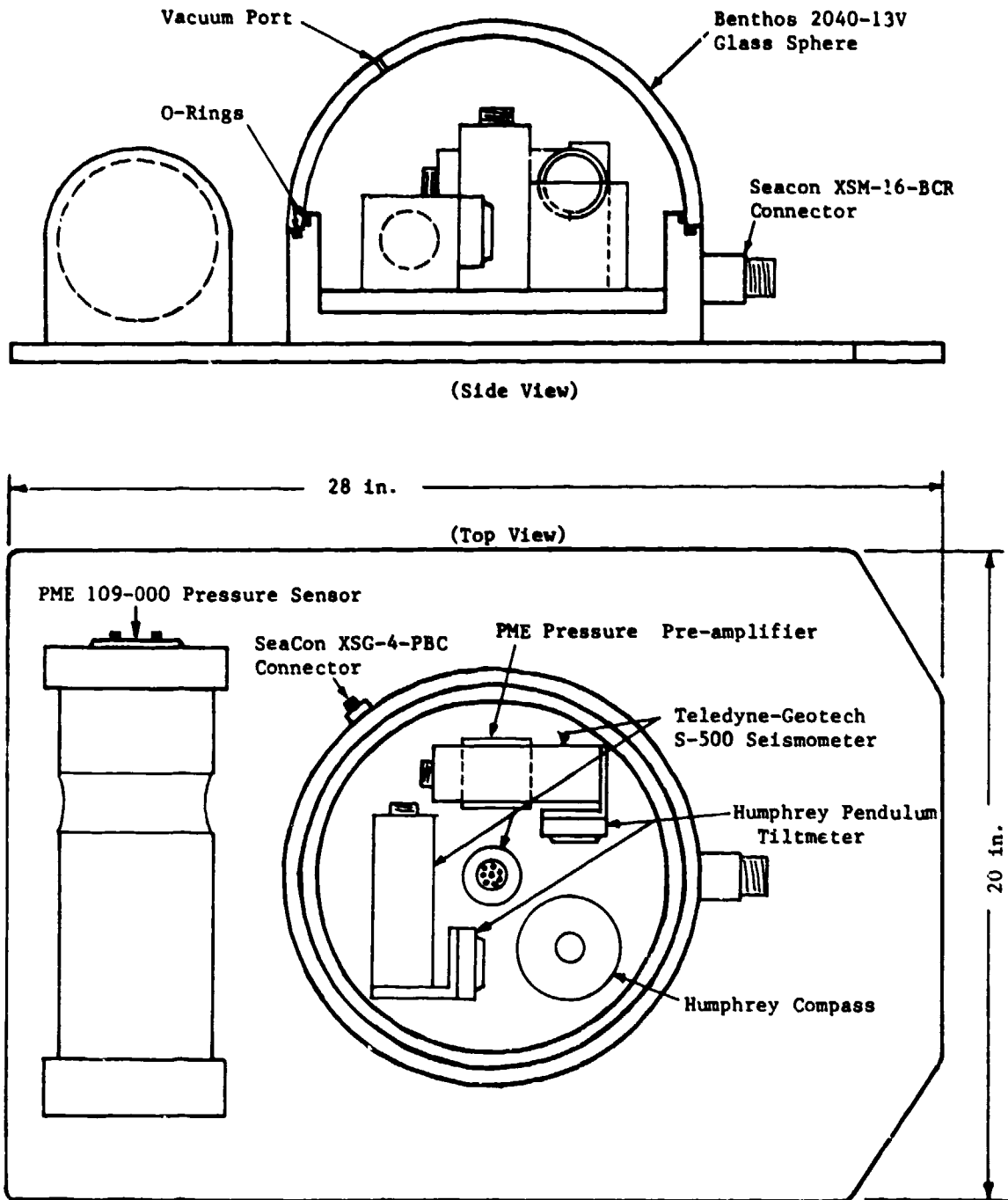


Figure 17. The waterproof housing and various instruments that comprise the Bottom Shear Modulus Profiler (from Ref. 39).

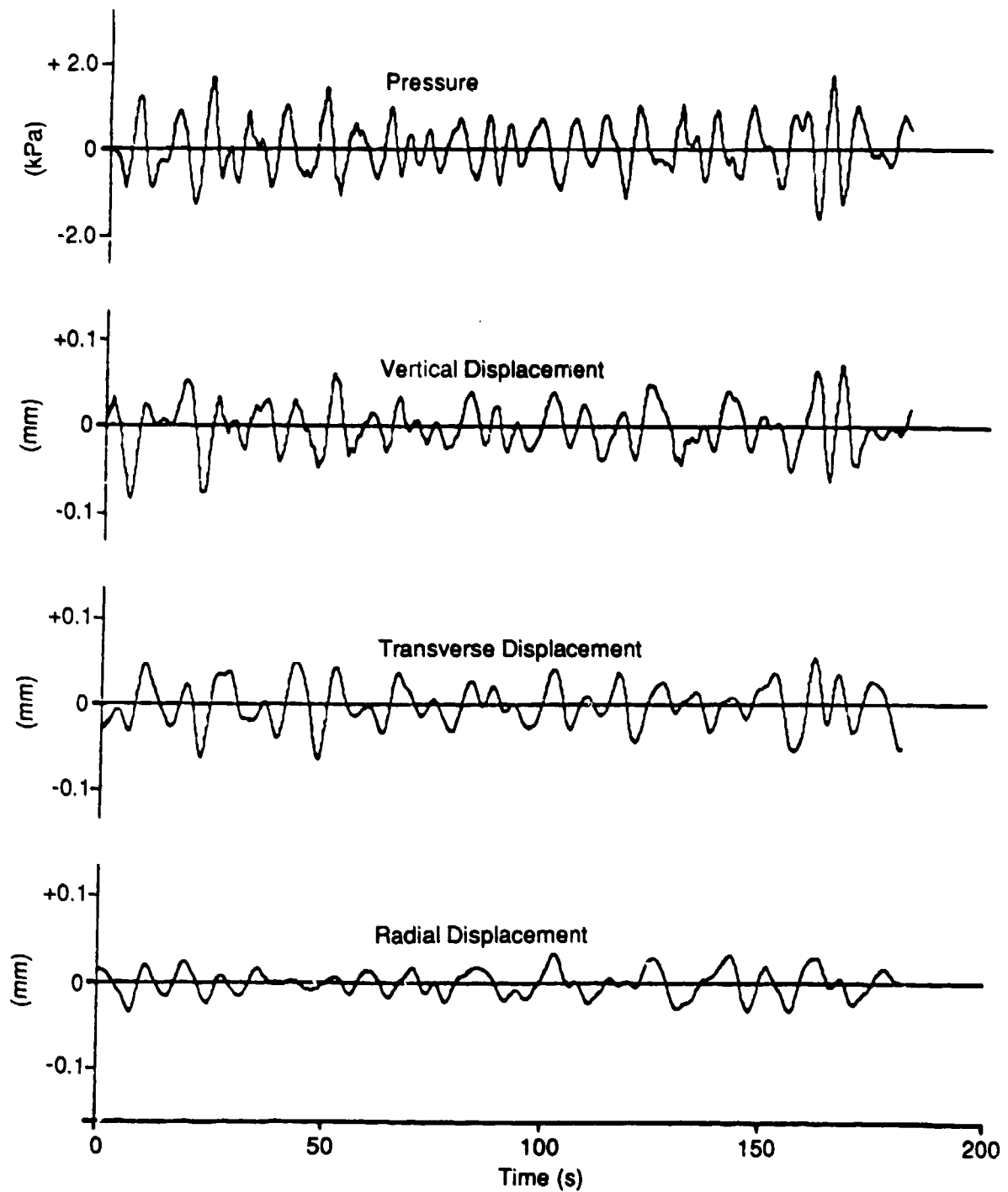


Figure 18. Sensitivity- and frequency-corrected BSMP time series. Seismometer velocity signals have been integrated to give displacements (from Ref. 39).

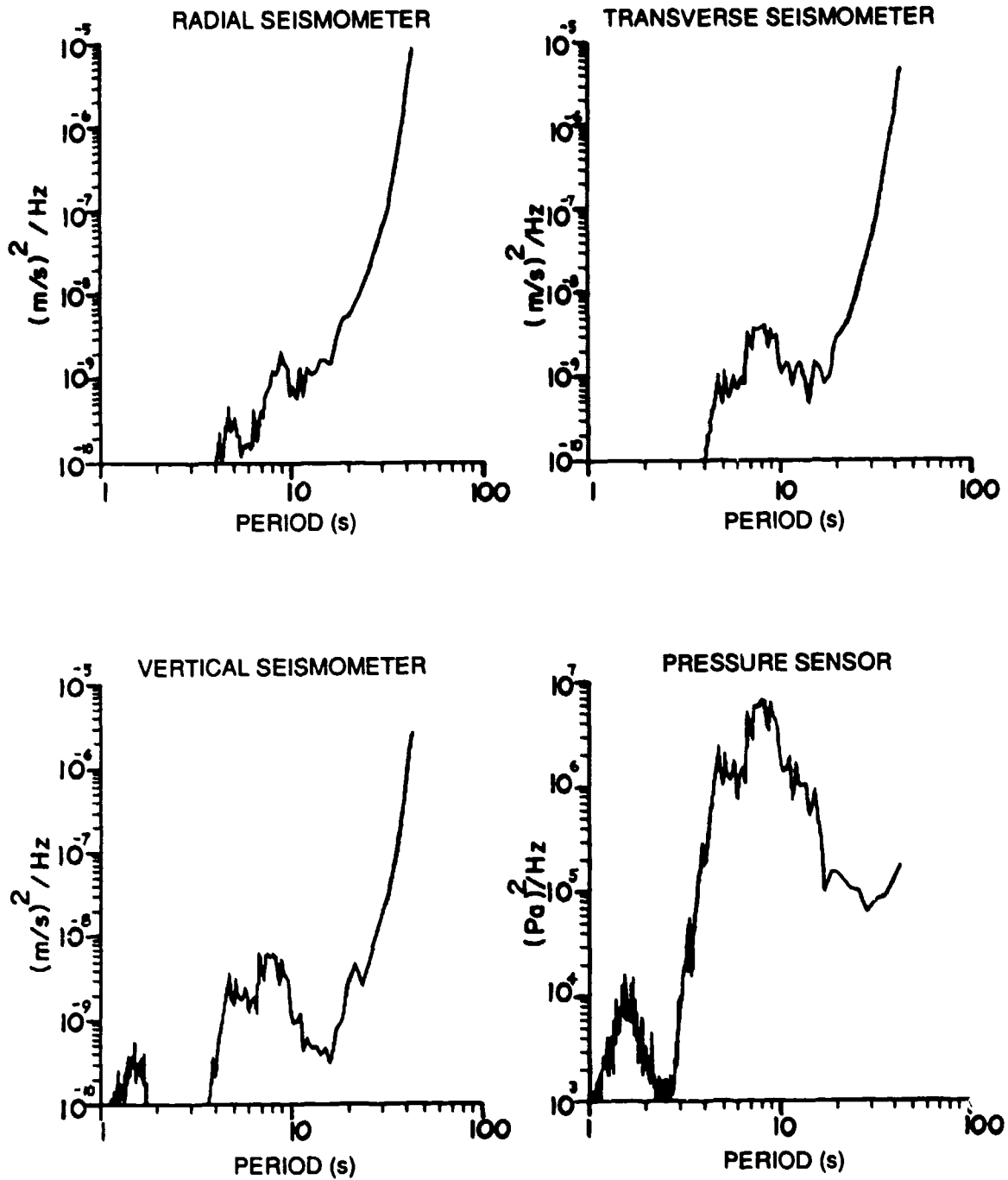


Figure 19. Frequency-corrected and time-averaged seismometer velocity and pressure power spectra from experiments 121_5 (from Ref. 39).

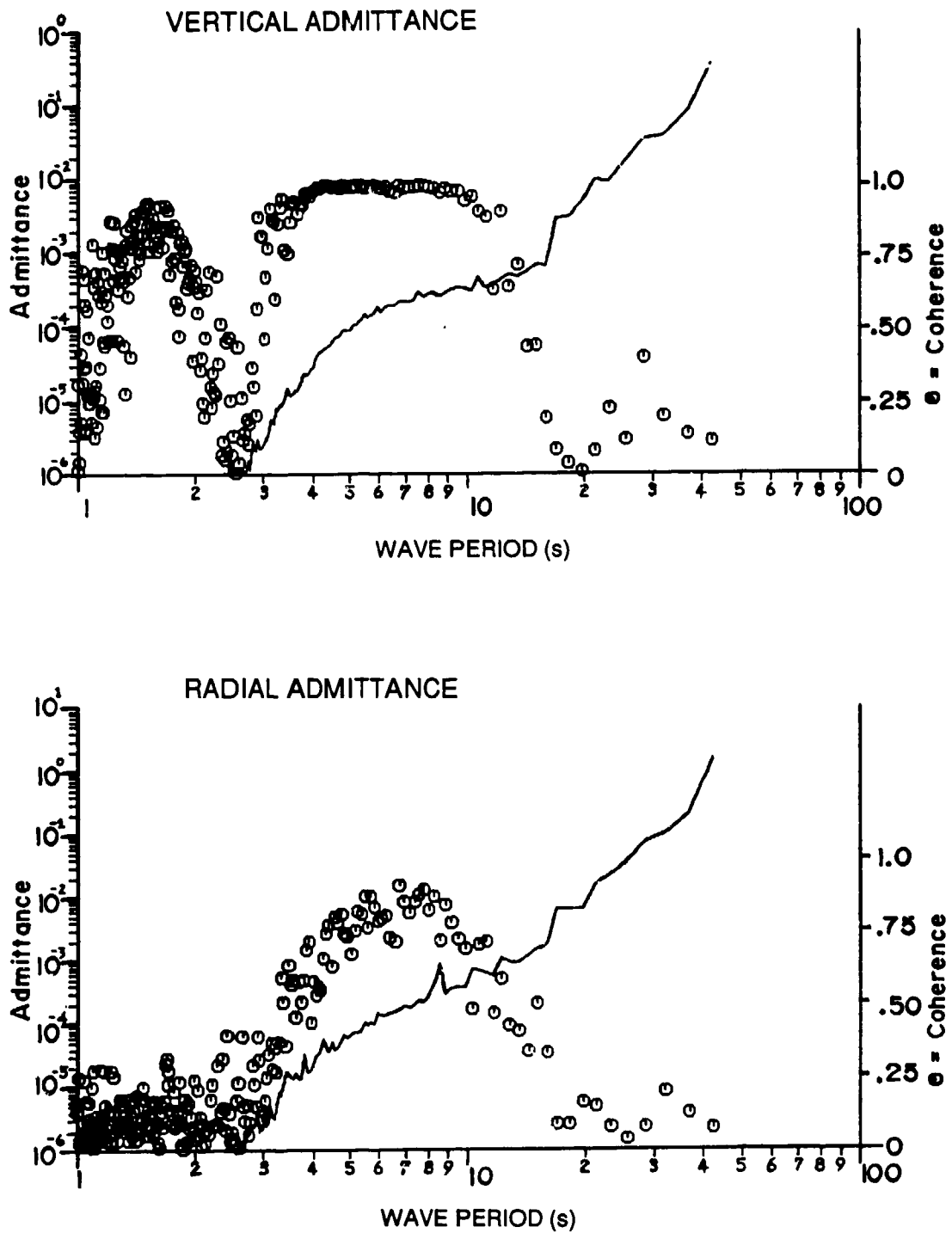


Figure 20. Vertical and radial admittance data with associated coherences versus wave period from experiment 121_5 (from Ref. 39).

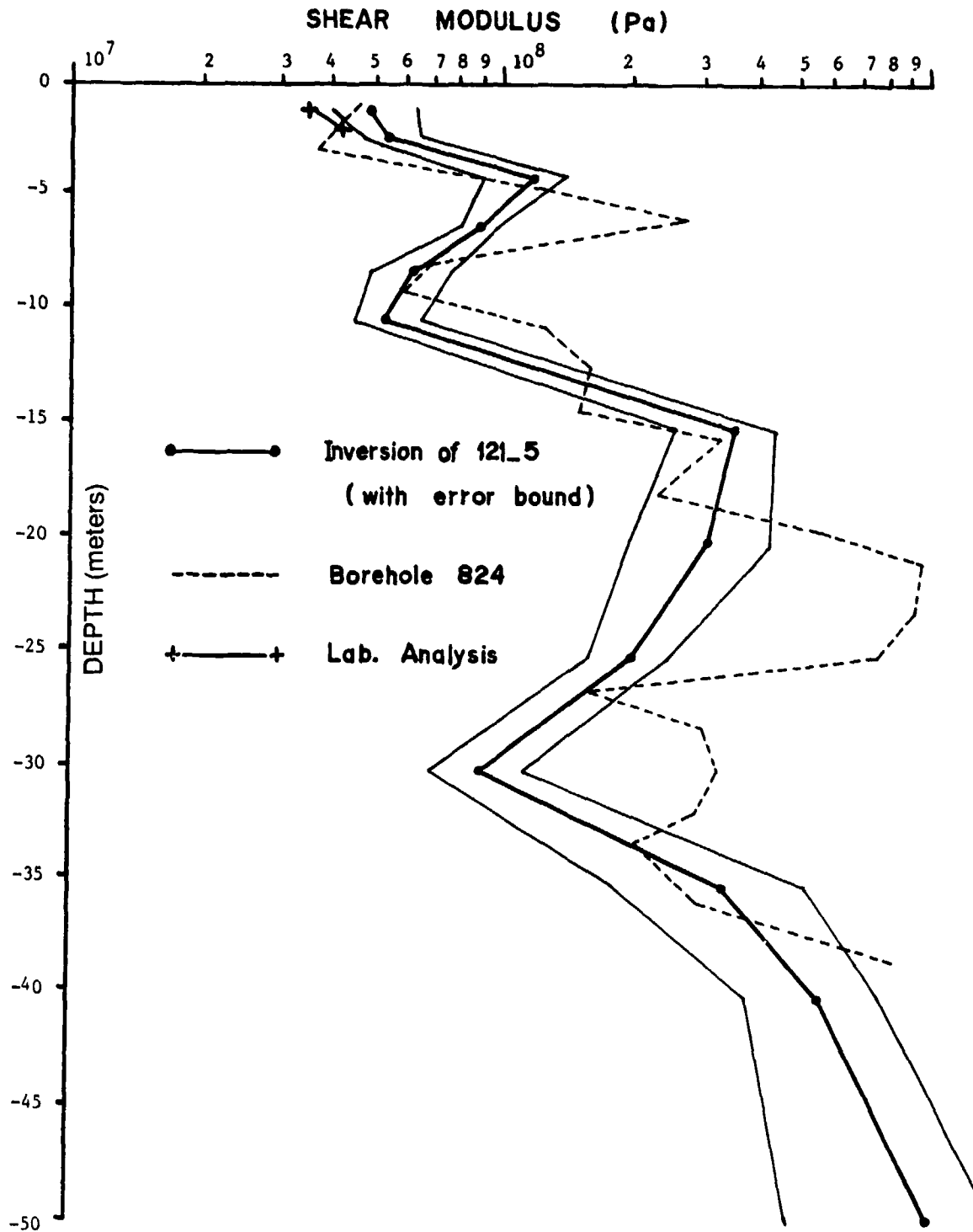


Figure 21. Comparison of inverted shear modulus profile from experiment 121_5 with reference data from a sediment shear strength borehole and laboratory analysis of a vibracore sample. The inversion used only vertical admittance data, and an eigenvalue expansion limit of 5 (from Ref. 39).

V. CONCLUSIONS

The methodology of geoacoustic and geophysical inversion techniques has now been developed and proven to the point that acoustical experiments and surveys in shallow water should use it on a regular basis. When the inversion methodology is combined with remote sensing instrumentation, we have a fast and efficient way to map the geoacoustic properties of the seabed as a function of depth.

For shallow water areas, the perturbative inverse technique based on measurements of the depth-dependent Green's function is adequate to construct the sound speed and attenuation profile of the compressional waves. Synthetic seismograms using a Biot geoacoustic model can be used to obtain interface losses resulting from compressional waves as well as porosity and permeability.

The study and measurement of seismic interface waves in the dispersive range of 0.1 to 0.025 s provide information on the shear wave properties of the bottom. In addition, it has been shown that ocean gravity swell waves of period 5 to 10 s provide data for the construction of accurate shear modulus profiles as a function of depth.

REFERENCES

1. M. Schulkin and J.A. Mercer, Low-frequency shallow water acoustics (20 to 500 Hz), APL-UW 8606, Applied Physics Laboratory, University of Washington, May 1986.
2. R.B. Lindsay, *Concepts and Methods of Theoretical Physics*, (D. Van Nostrand, New York, 1951) pp. 363-368. Also *Mechanical Radiation*, (McGraw-Hill Book Co., Inc., 1960) Chapter 12.
3. R.D. Stoll, "Acoustic waves in saturated sediments," in *Physics of Sound in Marine Sediments*, L. Hampton, Ed. (Plenum Press, New York, 1974) pp. 19-39.
4. T. Yamamoto, "Acoustic propagation in the ocean with a poro-elastic bottom," *J. Acoust. Soc. Am.* **73**, 1587-1596 (1983).
5. D. Rauch, "On the role of bottom interface waves in ocean seismo-acoustics: A review," in *Ocean Seismo-Acoustics: Low-Frequency Underwater Acoustics*, T. Akal and J.M. Berkson, Ed. (Plenum Press, New York, 1986) pp. 623-641.
6. T. Yamamoto and T. Torii, "Seabed shear modulus profile inversion using surface gravity (water) wave-induced bottom motion," *Geophys. J. R. Astr. Soc.* **85**, 413-431 (1986).
7. J.F. Lynch, G.V. Frisk, S.D. Rajan, G.J. Tango, M.F. Werby, A. Nagl, and H. Uberall, "Three related resonance methods for the determination of seafloor geoacoustic properties," in *Oceans 86*, Vol. 1, *Systems, Structures and Analysis*, 315-324 (IEEE Service Center, Piscataway, New Jersey 08854).
8. D.J. Thomson, "An inverse method for reconstructing the density and sound speed profiles of a layered ocean bottom," *IEEE Journal of Oceanic Engineering* **OE-9**, 18-25 (1984).

9. S.M. Candel, F. deFillipi, and A. Launay, "Determination of the inhomogeneous structure of a medium from its plane wave reflection response, Part I: A numerical analysis of the direct problem," *J. Sound Vib.* **68**, 571-582 (1980).

_____, "Determination of the inhomogeneous structure of a medium from its plane wave reflection response, Part II: A numerical approximation," *J. Sound Vib.* **68**, 583-595 (1980).
10. S.D. Rajan, "An inverse method for obtaining the attenuation profile and small variations in the sound speed and density profiles of the ocean bottom," WHOI-85-30, Ph. D. Dissertation, Woods Hole Oceanographic Institution, Woods Hole, Massachusetts, May 1985.
11. A. Nagl, H. Uberall, and W.R. Hoover, "Resonances in acoustic bottom reflection and their relation to the ocean bottom properties," *IEEE Trans. Geosci. and Rem. Sens.* **GE-20**, 332-337 (1982).
12. D.J. Thomson, "Inversion of ocean subbottom reflection data," in *Progress in Underwater Acoustics*, H.M. Merklinger, Ed. (Plenum Press, New York, 1986) pp. 271-278.
13. J.F. Lynch, S.D. Rajan, and G.V. Frisk, "A perturbative inverse method for the determination of geoacoustic parameters in shallow water," *IEEE Journal of Oceanic Engineering* **OE-9**, 287-294 (1984).
14. D.J. Thomson, "The determination of material properties of the sea-bed from the acoustic plane-wave reflection response," in *Acoustics and the Sea-Bed*, N.G. Pace, Ed. (Bath University Press, Bath, U.K., 1983) pp. 41-49.
15. A. Nagl, H. Uberall, and K.B. Yoo, "Acoustic exploration of ocean floor properties based on the ringing of sediment layer resonances," *Inverse Problems* **1**, 99-110 (1985).

16. S.D. Rajan and G.V. Frisk, "An inverse method for obtaining the attenuation profile and small variations in the sound speed and density profiles of the ocean bottom," *IEEE Journal of Oceanic Engineering* OE-9, 279-286 (1984).
17. S.D. Rajan, J.F. Lynch, and G.V. Frisk, "Perturbative inversion schemes to obtain bottom acoustic parameters in shallow water," *J. Acoust. Soc. Am.* **82**, 998-1017 (1987).
18. J.F. Lynch, S.D. Rajan, and G.V. Frisk, "A perturbative inverse method for the determination of geoacoustic parameters in shallow water," in *Progress in Underwater Acoustics*, H.M. Merklinger, Ed. (Plenum Press, New York, 1986) pp. 287-294.
19. E.L. Hamilton, "Geoacoustic modeling of the seafloor," *J. Acoust. Soc. Am.* **68**, 1313-1340 (1980).
20. S.D. Rajan and J.F. Lynch, personal communication, September 1987.
21. M.F. Werby, G.J. Tango, and H.B. Ali, "A synthetic aperture array technique for fast approximate geobottom reconnaissance," *IEEE Journal of Oceanic Engineering* OE-9, 295-302 (1984).
22. M.F. Werby, G.J. Tango, and H.B. Ali, "A synthetic aperture-array technique for fast approximate geobottom reconnaissance," in *Progress in Underwater Acoustics*, H.M. Merklinger, Ed. (Plenum Press, New York, 1986) pp. 295-302.
23. M.F. Werby and G.J. Tango, "Characterization of average geoacoustic bottom properties from expected propagation behavior at very low frequencies (VLF) using a towed array simulation," in *Ocean Seismo-Acoustics Low-Frequency Underwater Acoustics*, T. Akal and J.M. Berkson, Ed. (Plenum Press, New York, 1986) pp. 881-889.

24. T. Akal and F.B. Jensen, "Effects of the sea-bed on acoustic propagation," in *Acoustics and the Sea-Bed*, N.G. Pace, Ed. (Bath University Press, Bath, U.K., 1983) pp. 225-232.
25. D. Rauch and B. Schmalfeldt, "Ocean-bottom interface waves of the Stoneley/Scholte type: Properties, observations and possible use," in *Acoustics and the Sea-Bed*, N.G. Pace, Ed. (Bath University Press, Bath, U.K., 1983) pp. 307-316.
26. R.M. Holt, J.M. Hovem, and J. Syrstad, "Shear modulus profiling of near bottom sediments using boundary waves," in *Acoustics and the Sea-Bed*, N.G. Pace, Ed. (Bath University Press, Bath, U.K., 1983) pp. 317-325.
27. P.I. Vidmar and T.L. Foreman, "A plane-wave reflection loss model including sediment rigidity," *J. Acoust. Soc. Am.* **66**, 1830-1847 (1979).
28. J. Dorman, "Period equation for waves of Rayleigh type on a layered, liquid-solid half space," *Bull. Seismol. Soc. Am.* **52**, 389-397 (1962).
29. F.B. Jensen and H. Schmidt, "Shear properties of ocean sediments determined from numerical modelling of Scholte wave data," in *Ocean Seismo-Acoustics: Low-Frequency Underwater Acoustics*, T. Akal and J.M. Berkson, Ed. (Plenum Press, New York, 1986) pp. 683-692.
30. E. Strick and A.S. Ginzburg, "Stoneley-wave velocities for a fluid-solid interface," *Bull. Seismol. Soc. Am.* **46**, 281-292 (1956).
31. W.M. Ewing, W.S. Jardetzky, and F. Press, *Elastic Waves in Layered Media* (McGraw-Hill Book Co., Inc., New York, NY, 1957).
32. R.D. Stoll, "Marine sediment acoustics," *J. Acoust. Soc. Am.* **77**, 1789-1799 (1985).

33. B. Schmalfeldt and D. Rauch, "Explosion-generated seismic interface waves in shallow water: experimental results," Report SR-71, SACLANT ASW Research Centre, La Spezia, Italy (1983). [AD A 135 551]
34. H. Schmidt and F.B. Jensen, "Efficient numerical solution technique for wave propagation in horizontally stratified ocean environments," Report SM-173, SACLANT ASW Research Centre, La Spezia, Italy (1984). [AD A 148 537]
35. H. Schmidt, "Excitation and propagation of interface waves in a stratified sea-bed," in *Acoustics and the Sea-Bed*, N.G. Pace, Ed. (Bath University Press, Bath, U.K., 1983) pp. 327-334.
36. H.W. Kutschale, "Rapid computations by wave theory of propagation loss in the Arctic Ocean," Columbia University, Palisades, New York, CU-8-73 (1973).
37. F.R. DiNapoli and R. L. Deavenport, "Theoretical and numerical Green's function field solution in a plane multilayered medium," *J. Acoust. Soc. Am.* **67**, 92-105 (1980).
38. A. Turgut and T. Yamamoto, "Synthetic seismograms for marine sediments and determination of porosity and permeability," *Geophysics* (in press).
39. M. Trevorrow, T. Yamamoto, M. Badiy, A. Turgut, and C. Conner, "Experimental verification of seabed shear modulus profile inversions using surface gravity (water) wave-induced seabed motion," *Geophys. J. R. Astr. Soc.* (in press).
40. J.F. Claerbout, "Synthesis of a layered medium from its acoustic transmission response," *Geophysics* **33**, 264-269 (1968).
41. G. Kunetz, "Generalization des operateurs d'anteresonance a nombre quelconque de reflecteurs," *Geophys. Prop.* **12**, 283-289 (1964).

42. P. Goupillaud, "An approach to inverse filtering of near-surface layer effects from seismic records," *Geophysics* **26**, 754-760 (1961).
43. H. Deresiewicz and A. Levy, "The effect of boundaries on wave propagation in a liquid-filled porous solid," *Bull. Seismol. Soc. Am.* **57**, 381-391 (1967).
44. D. C. Ganley, "A method for calculating synthetic seismograms which include the effects of absorption and dispersion," *Geophysics* **46**, 1100-1107 (1981).
45. W. I. Futterman, "Dispersive body waves," *J. Geophys. Res.* **69**, 5279-5291 (1962).
46. M. A. Biot, "Mechanics of deformation and acoustic propagation in porous media," *J. Appl. Phys.* **33**, 1482-1498 (1962).
47. M. A. Biot, "Generalized theory on acoustic propagation in porous dissipative media," *J. Acoust. Soc. Am.* **34**, 1254-1264 (1962).
48. D. D. Jackson and D. L. Anderson, "Physical mechanics of seismic wave attenuation," *Rev. Geophys. Space Phys.* **8**, 1-63 (1970).
49. T. J. Plona and D. L. Johnson, "Acoustic properties of porous systems: I. Phenomenological description," in *Physics and Chemistry of Porous Media*, D. L. Johnson and P. N. Sen, Ed., American Institute of Physics (1984), pp. 89-104.
50. T. Yamamoto, "On the response of a Coulomb-damped poro-elastic bed to water waves," *Mar. Geotech.* **5**, 93-130 (1983).
51. T. Yamamoto, S. Takahashi, and B. Schuckman, "Physical modelling of seafloor interactions," *J. Engr. Mech., Am. Soc. Civ. Engrs.* **109**, 54-72 (1983).
52. T. Yamamoto and B. Schuckman, "Experiments and theory of wave-soil interactions," *J. Engr. Mech., Am. Soc. Civ. Engrs.* **110**, 95-112 (1984).

53. T. Yamamoto, "Numerical integration method for seabed response to water waves," *J. Soil Dynam. Earthq. Engr.* **2**, 92-100 (1983).
54. M. V. Trevorrow, M. Badiy, A. Turgut, C. Conner, and T. Yamamoto, "A quantitative analysis of seabed shear modulus inversions from experiments on the New Jersey shelf in August, 1986," R.S.M.A.S./Univ. of Miami technical report 87-003 (1987).
55. T. Yamamoto, M. Badiy, C. Conner, A. Turgut, and M. Trevorrow, "Bottom shear modulus profiler (BSMP) experiments on the New Jersey shelf in August, 1986," R.S.M.A.S./Univ. of Miami technical report 86-009 (1986).

Appendix A

Summary of Inverse Theory for Bottom Shear Modulus Profiles*

*This present summary has been adapted from Yamamoto and Torii^{A-1} with the authors' kind permission.

I. LINEAR INVERSE THEORY

The linear inverse problem most often encountered in geophysics can be formulated as

$$e_i = \int_I C_i(y) m(y) dy \quad (i = 1, 2, 3, \dots, N) \quad (\text{A-1})$$

or, in the computationally simpler discrete form,

$$e_i = \sum_{j=1}^M C_{ij} m_j \quad (i = 1, 2, 3, \dots, N). \quad (\text{A-2})$$

In matrix notation

$$e = Cm, \quad (\text{A-3})$$

where e_i is one of N observations (DATA), C is a kernel derived from theory, and m is the unknown function (MODEL) defined on the I interval.^{A.2-A.4}

The singular value decomposition of matrix C is used to solve equation (A-3) following Lanczos,^{A.5}

$$C = U\Lambda V^T. \quad (\text{A-4})$$

U_i : the columns of U are the N -dimensional eigenvectors of a coupled eigenvector-eigenvalue problem that spans the data space. V_i : the columns of V are the M -dimensional eigenvectors of a coupled eigenvector-eigenvalue problem which spans the solution (MODEL) space. Λ is the diagonal matrix with the corresponding eigenvalues λ_i , which are sorted into descending order. Zero-valued eigenvectors are not included. This leads to

$$\begin{aligned} CC^T U_i &= \lambda_i^2 U_i \quad (i = 1, 2, \dots, N), \\ C^T C V_i &= \lambda_i^2 V_i \quad (i = 1, 2, \dots, M), \end{aligned} \quad (\text{A-5})$$

and the U_i and V_i are orthonormal such that

$$U_i^T U_j = \delta_{ij}, \quad V_i^T V_j = \delta_{ij}. \quad (\text{A-6})$$

In terms of U , V , and Λ , the solution to equation (A-3) is

$$\begin{aligned} \hat{m} &= C^{-1}e \\ &= V\Lambda^{-1}U^T e \\ &= \sum_{i=1}^N \frac{U_i \cdot e}{\lambda_i} V_i. \end{aligned} \quad (\text{A-7})$$

For the data with noise, the following is considered for the construction of the solution using the truncated singular value expansion,

$$\hat{m} = \sum_{i=1}^L \frac{U_i \cdot e}{\lambda_i} V_i \quad (L < N). \quad (\text{A-8})$$

There are good reasons for using the truncated expansion. With the assumption of Gaussian white noise, one can show that the uncertainty of each coefficient multiplying V_i in equation (A-7) is proportional to $\lambda_i^{-1/2}$. Thus, the expansion equation (A-7) is in terms of vectors whose coefficients increase in uncertainty. It is also usually the case that the vectors V_i become more oscillatory as i increases (exceptions to this rule are very rare). Thus, the truncated expansion equation (A-8) simultaneously removes those parts of the solution that are sensitive to noise and gives a smoothed estimate of the solution. This point is demonstrated here using synthetic data without noise and measured data with noise.

The *resolution matrix* has been adopted to determine the quality of the above solution using the truncated singular value expansion

$$C^{-1}C = \sum_{k=1}^L V_{ik} \cdot V_{kj}. \quad (\text{A-9})$$

In the ideal case in which $C^{-1}C$ results in the identity matrix, the resolution is perfect. When $C^{-1}C$ has near unity values on the diagonal and small values elsewhere, the computed solution represents a smoothed version of the true solution.

II. NONLINEAR INVERSE PROBLEM

All of the above analyses apply to the linear inverse problem. *For the nonlinear problem such as the one under consideration, an iterative linearization scheme has been used by which successive approximations to the model can be computed.* Starting with the nonlinear relation between data e and model m , and recalling equation (A-3),

$$e = f(m). \quad (\text{A-10})$$

In order to minimize $\phi = |e - f(m_0)|^2$, it is necessary to assume an initial value m_0 and then linearize. Expanding equation (A-10) in a Taylor series form results in

$$e = f(m) \approx f(m_0) + \left(\frac{\partial f(m)}{\partial m} \right)_{m=m_0} (m - m_0) \quad (\text{A-11})$$

or

$$\begin{aligned}
 e - f(m_0) &= \left(\frac{\partial f(m)}{\partial m} \right)_{m=m_0} (m - m_0) \\
 &= \left(\frac{f(m + \Delta m) - f(m)}{\Delta m} \right)_{m=m_0} (m - m_0). \quad (\text{A-12})
 \end{aligned}$$

The derivatives $\partial f / \partial m$ are approximated by finite differences in the last equation. As Yamamoto shows, the finite difference approximations to the derivatives are quite good for our problem. His model and parameters allow him to arrive at the following matrix equation:

$$\Delta e = C \Delta m . \quad (\text{A-13})$$

The linear system expressed by equation (A-13) is solved for Δm using equation (A-8) and then repeating the process after replacing m_0 by $m_0 + \Delta m$. This process is repeated until Δm becomes acceptably small. In practice the method does not always converge. A serious shortcoming of this linearization-iteration approach is that even when a solution is found it is not possible to say without testing whether another equally acceptable (but well separated in model space) model exists.

When problems are treated as nonlinear it is found that only the second, third, or fourth terms are retained for the first few iterations, but when approaching the final solution the solution retains more terms.

REFERENCES - APPENDIX A

- A.1. T. Yamamoto, and T. Torii, "Seabed shear modulus profile inversion using surface gravity (water) wave-induced bottom motion," *Geophys. J.R. Astr. Soc.* **85**, 413-431 (1986).
- A.2. K. Aki and P. G. Richards, *Quantitative Seismology: Theory and Methods*, Vols. 1 and 2 (W. H. Freeman, New York, 1980).
- A.3. M. G. Brown, "Linearized travel time, intensity and waveform inversions in the ocean sound channel — a comparison," *J. Acoust. Soc. Am.* **75**, 1451-1461 (1984).
- A.4. W. Menke, *Geophysical Data Analysis: Discrete Inverse Theory* (Academic Press, New York, 1984).
- A.5. C. Lanczos, *Linear Differential Operators* (Van Nostrand, London, 1961) Chapter 3.

UNCLASSIFIED

SECURITY CLASSIFICATION OF THIS PAGE (When Data Entered)

A192 107

REPORT DOCUMENTATION PAGE		READ INSTRUCTIONS BEFORE COMPLETING FORM
1. REPORT NUMBER APL-UW 8711	2. GOVT ACCESSION NO.	3. RECIPIENT'S CATALOG NUMBER
4. TITLE (and Subtitle) Remote Sensing of Acoustic Properties of Shallow Water Sediments: A Review		5. TYPE OF REPORT & PERIOD COVERED
7. AUTHOR(s) M. Schulkin		6. PERFORMING ORG. REPORT NUMBER APL-UW 8711
9. PERFORMING ORGANIZATION NAME AND ADDRESS Applied Physics Laboratory University of Washington 1013 NE 40th Street Seattle, WA 98105		8. CONTRACT OR GRANT NUMBER(s) N00014-84-K-0646/A00004
11. CONTROLLING OFFICE NAME AND ADDRESS Office of Naval Research (Code 425UA) 800 N. Quincy Street Arlington, VA 22217		10. PROGRAM ELEMENT, PROJECT, TASK AREA & WORK UNIT NUMBERS
14. MONITORING AGENCY NAME & ADDRESS (if different from Controlling Office)		12. REPORT DATE September 1987
		13. NUMBER OF PAGES 57
		15. SECURITY CLASS. (of this report) UNCLASSIFIED
		15a. DECLASSIFICATION/DOWNGRADING SCHEDULE
16. DISTRIBUTION STATEMENT (of this Report) Approved for public release; distribution unlimited.		
17. DISTRIBUTION STATEMENT (of the abstract entered in Block 20, if different from Report)		
18. SUPPLEMENTARY NOTES		
19. KEY WORDS (Continue on reverse side if necessary and identify by block number)		
Remote Sensing Shallow Water Acoustics Shallow Water Sediments Inverse Methods	Biot Geophysical Parameters Sediment Compressional Waves Sediment Shear Waves Seismic Interface Waves	Sediment Porosity Sediment Permeability Sediment Shear Modulus
20. ABSTRACT (Continue on reverse side if necessary and identify by block number)		
<p>A review is presented of remote sensing methods and associated inverse procedures for obtaining the acoustic properties of sediments in shallow water. The properties of interest are the vertical profiles of density, compressional wave velocity and attenuation, and shear wave velocity and attenuation. For compressional waves, the remotely sensed information required is the modal reflection coefficient of the seabed, usually expressed in terms of the depth-dependent Green's function at specific locations in the water column. For shear waves, information about the Scholte and Rayleigh interface waves on the seabed is necessary. Also reviewed are methods for remote sensing of the Biot geophysical parameters, shear modulus, permeability, and porosity, from which geoaoustic properties can be derived.</p>		

DD FORM 1473
1 JAN 73EDITION OF 1 NOV 65 IS OBSOLETE
S/N 0102-LF-014-6601

UNCLASSIFIED

SECURITY CLASSIFICATION OF THIS PAGE (When Data Entered)